



Preclinical cardiac safety assessment of pharmaceutical compounds using an integrated systems-based computer model of the heart

Dean Bottino^a, R. Christian Penland^b, Andrew Stamps^c,
Martin Traebert^d, Bérengère Dumotier^d, Anna Georgieva^e,
Gabriel Helmlinger^f, G. Scott Lett^a

^a*The BioAnalytics Group LLC, USA*

^b*Predix Pharmaceuticals, USA*

^c*Department of Chemical Engineering, University of South Carolina, USA*

^d*Safety Profiling & Assessment, Novartis Pharma AG, Basel, Switzerland*

^e*Modeling & Simulation, Novartis Pharmaceuticals, East Hanover, USA*

^f*Modeling & Simulation, Novartis Institutes for Biomedical Research Inc., Cambridge, USA*

Available online 7 July 2005

Abstract

Blockade of the delayed rectifier potassium channel current, I_{K_r} , has been associated with drug-induced QT prolongation in the electrocardiogram and life-threatening cardiac arrhythmias. However, it is increasingly clear that compound-induced interactions with multiple cardiac ion channels may significantly affect QT prolongation that would result from inhibition of only I_{K_r} [Redfern, W.S., Carlsson, L., et al., 2003. Relationships between preclinical cardiac electrophysiology, clinical QT interval prolongation and torsade de pointes for a broad range of drugs: evidence for a provisional safety margin in drug development. *Cardiovasc. Res.* 58(1), 32–45]. Such an assessment may not be feasible in vitro, due to multifactorial processes that are also time-dependent and highly non-linear.

Limited preclinical data, I_{K_r} hERG assay and canine Purkinje fiber (PF) action potentials (APs) [Gintant, G.A., Limberis, J.T., McDermott, J.S., Wegner, C.D., Cox, B.F., 2001. The canine Purkinje fiber: an in vitro model system for acquired long QT syndrome and drug-induced arrhythmogenesis. *J. Cardiovasc. Pharmacol.* 37(5), 607–618], were used for two test compounds in a systems-based modeling

platform of cardiac electrophysiology [Muzikant, A.L., Penland, R.C., 2002. Models for profiling the potential QT prolongation risk of drugs. *Curr. Opin. Drug. Discov. Dev.* 5(1), 127–35] to: (i) convert a canine myocyte model to a PF model by training functional current parameters to the AP data; (ii) reverse engineer the compounds' effects on five channel currents other than I_{Kr} , predicting significant IC_{50} values for $I_{Na^+,sustained}$ and $I_{Ca^{2+},L-type}$, which were subsequently experimentally validated; (iii) use the predicted ($I_{Na^+,sustained}$ and $I_{Ca^{2+},L-type}$) and measured (I_{Kr}) IC_{50} values to simulate dose-dependent effects of the compounds on APs in endocardial, mid-myocardial, and epicardial ventricular cells; and (iv) integrate the three types of cellular responses into a tissue-level spatial model, which quantifiably predicted no potential for the test compounds to induce either QT prolongation or increased transmural dispersion of repolarization in a dose-dependent and reverse rate-dependent fashion, despite their inhibition of I_{Kr} in vitro.

© 2005 Published by Elsevier Ltd.

Contents

1. Introduction	416
1.1. Drug-induced arrhythmia and preclinical safety assessment	416
1.2. Review of applicable experimental methods	417
1.2.1. Ion channels	417
1.2.2. Purkinje fiber assay	418
1.2.3. Dispersion of repolarization	419
1.2.4. Electrocardiogram	419
1.3. Modeling methodologies applicable to safety assessment	420
2. Methods	421
2.1. Experimental methods	421
2.1.1. Preparation of guinea pig ventricular myocytes	421
2.1.2. Patch-clamp measurements for hERG, L-type Ca^{2+} and Na^+ currents	421
2.2. Mathematical modeling methods	422
2.2.1. Simulation of the canine wedge transmural electrocardiogram	422
2.2.2. Simulation of drug effects on repolarization	423
2.3. Rapid development of a Purkinje fiber model	423
2.3.1. Estimation of ion-channel pharmacology from action potential measurements	423
2.3.2. Data preprocessing	424
2.3.3. Optimization	424
2.3.4. Error metrics	424
3. Results	425
3.1. Experimental results	425
3.1.1. COMPOUND A and COMPOUND B	425
3.1.2. Summary	426
3.2. Modeling results	428
3.2.1. Rapid prototyping of a Purkinje fiber model from a canine ventricular myocyte model	428
3.2.2. IC_{50} predictions for COMPOUND A and COMPOUND B	429
3.2.3. Forward predictions of action potentials in isolated myocytes	430
3.2.4. Transmural electrocardiogram and dispersion of repolarization	433
4. Discussion	435
4.1. Toward a simulation-assisted integrated non-clinical safety assessment process	437
. Editor's note	439
References	439

1. Introduction

1.1. Drug-induced arrhythmia and preclinical safety assessment

Drug-induced QT prolongation and the accompanying pro-arrhythmic risk are major regulatory concerns in drug development, contributing to half of the safety-related withdrawals of drugs from the market since 1997 and impacting all therapeutic drug classes (Redfern et al., 2003). The QT interval of the electrocardiogram (ECG) marks the duration of time between ventricular depolarization and repolarization. Drugs that delay ventricular repolarization and prolong the QT interval are associated with an increased risk of life-threatening ventricular tachyarrhythmia, in particular Torsades de Pointes (TdP).

Cardiac repolarization is a complex physiological process terminating the cardiac action potential (AP), and it results from the activities of multiple membrane ion channels and transporters. These ion channels and transporters interact through membrane potential and intra-/extracellular ionic concentrations, but are also affected by systemic factors including hormone regulation, metabolic state, and autonomic nervous tone. It is therefore no surprise that a variety of mechanisms could contribute to abnormal repolarization in the heart.

Prolongation of the AP can result from increases in inward currents (Na^+ or Ca^{2+}) or from inhibition of one or more of the outward K^+ currents. Most drugs initially discovered to prolong the QT interval are class III anti-arrhythmics that block K^+ currents. It is now widely accepted that the blockade of I_{Kr} current by these drugs is at least in part responsible for their pro-arrhythmic effect; however, this risk may be modulated by blocking other channels (Curtis et al., 2003). Despite the documented risk and increasing regulatory awareness, 23% of US adult outpatients are prescribed at least one drug known to have pro-arrhythmic risk, i.e., having an official warning for QT prolongation or TdP, or with published data on QT prolongation, ventricular tachycardia, or class III effect Food and Drug Administration (FDA, 2003, 2004a, b). Accurately assessing the pro-arrhythmic potential of drug candidates should be done early in preclinical development to avoid the economic and public health consequences of late stage failures of drug candidates, unfavorable labeling, and withdrawals of FDA-approved products.

Although a variety of in vitro and in vivo experimental models are available for assessing the QT prolongation and pro-arrhythmic potential of a drug candidate, no single preclinical model has been proven to be a predictive surrogate for the human heart, i.e., clinical exposure (Hammond et al., 2001). Recognizing this need, pharmaceutical regulatory agencies worldwide together with industry and academic scientists have developed guidance urging the integration of several assays in hopes that their combination will provide a superior measure of true pro-arrhythmic risk (S7B-FDA, 2004). In a realistic development environment, the earliest indications of pro-arrhythmic risk are commonly predicted using assays for I_{Kr} inhibition and an AP assay. This paper presents a novel computational system that uses only these two assay results to predict key electrophysiological markers used in the early cardiac safety assessment of compounds. These quantities of interest are: (i) drug effects on multiple cardiac ion-channel currents; (ii) multiple features of compound effects on Purkinje and ventricular myocyte AP, with quantitative spatial distinction for endocardial, mid-myocardial (M) and epicardial (Epi) cells across the ventricular wall; and (iii) changes in ECG accounting for multiple patient risk factors.

Using two candidate compounds in development, the computational system was tested as a tool to aid in the cardiac safety assessment. These two compounds showed significant I_{Kr} blockade, but lacked the dose-dependent prolongation of AP commonly associated with compounds that block I_{Kr} . The computational system was used, first to provide a mechanistic explanation of these two results, and second to predict the clinical implications of the ion-channel mechanisms of the compounds.

1.2. Review of applicable experimental methods

1.2.1. Ion channels

Several potassium currents are involved in the process of cardiac repolarization (Tristani-Firouzi et al., 2001). In this finely tuned mechanism, the rapidly activating delayed rectifier current I_{Kr} has been demonstrated to play a major role (Sanguinetti et al., 1995a). The pore forming protein of the I_{Kr} current (the α -subunit encoded by the human ether-a-gogo-related gene or hERG, see Sanguinetti et al., 1995b) is known to be a common target of compounds which are able to prolong the ventricular repolarization process in humans with the acquired long QT syndrome (LQTS), and also the site of several mutations responsible for the loss of function of this channel in human congenital LQTS (LQT2; Curran et al., 1995).

Recent data have shown that the coexpression of the hERG α -subunit with minK related protein (MiRP1) reconstitutes the native cardiac I_{Kr} (Abbott et al., 1999) and that the presence of this additional subunit can impact the pharmacological sensitivity to certain inhibitors. Still, other studies have demonstrated that the inhibitory effects of several potent I_{Kr} blockers on the hERG current were not altered by the presence of MiRP1 (Kamiya et al., 2001; Scherer et al., 2002; Weerapura et al., 2002). While important to the ongoing understanding of cardiac repolarization, these discrepancies have not proved sufficient to alter the prevalence of hERG inhibition studies (without MiRP1) in the pharmaceutical development industry. Therefore, data in this study are derived from heterologous cell lines expressing only the hERG α -subunit. When stably transfected in HEK293 cells, hERG offers the opportunity to directly check the ability of a new compound entity (NCE) to reduce the current generated by this pore forming protein and therefore, to indirectly estimate the potential risk associated with inadequate cardiac repolarization. This risk is quantified by the calculation of an IC_{50} value, i.e., the drug concentration that reduces the maximum hERG tail current by 50%. It is now generally accepted that potent hERG blockers display IC_{50} values of $\leq 1 \mu\text{M}$, while the weakest ones are associated with IC_{50} values of $> 10 \mu\text{M}$.

It has been shown that a large number of compounds known to induce TdP in humans have been shown to block hERG current with an IC_{50} in the low micromolar range (Redfern et al., 2003). The hERG assay by itself is not sufficient to clearly predict the pro-arrhythmic potential of NCEs; however, the assay can be used as a profiling tool for early development drug candidates by generating the IC_{50} value for each compound and then ranking the drugs according to these IC_{50} values. Generally, the patch-clamp technique can also be used to quantify the interaction of NCE with other types of ion channels. For instance, assessing the drug effects on the fast inward sodium current or the L-type calcium current helps to better understand the effects of a drug at the cellular level.

1.2.2. Purkinje fiber assay

Measurements of transmembrane APs permit the prediction, characterization, or understanding of the cellular ion mechanisms underlying pro-arrhythmic effects. Action potential duration (APD) recordings are performed in multi-cellular preparations and form the basis for the detection and quantification of APD prolongation and early afterdepolarizations (EADs) which are considered cellular-level events initiating arrhythmias (El-Sherif et al., 1997; January and Shorofsky, 1990; Verduyn et al., 1997a, b; Yan et al., 2001). EADs are cellular depolarizations, which may develop during the plateau (phase 2 of AP) or during the final repolarization (phase 3 of AP) of the AP. EAD development is the consequence of an exaggerated APD prolongation that keeps the membrane potential at values allowing spontaneous generation of net inward currents (the Na^+ “window”) or slowly inactivating currents such as the L-type Ca^{2+} current, the T-type Ca^{2+} current, the transient inward current (I_{TI}), or the Na^+ – Ca^{2+} exchange current (January and Riddle, 1989; January and Moscucci, 1992). Such spontaneous depolarizations may lead to premature APs or even bursts of potentials known as triggered activity (January et al., 1991).

AP recording can be used efficiently in detecting drug-induced APD prolongation and subsequent EADs, assuming several experimental conditions are met, such as physiological concentrations of different ions (Na^+ , Ca^{2+} , K^+). Indeed, electrolyte imbalance is known to impair cardiac electrogenesis and to favor arrhythmia in vivo. Therefore, additional experimental protocols may use lower K^+ ion concentration in order to promote EADs and, conversely, higher K^+ ion concentration to suppress these particular events (Roden, 1993; Puisieux et al., 1996). In well-designed experimental protocols, preparations are challenged with different stimulation rates, especially low rates (<1 Hz), which are known to favor the emergence of EADs, both in in vitro and in vivo models (Davidenko et al., 1989; El-sherif et al., 1997; Dumotier et al., 1999).

Purkinje fibers (PFs) are widely used for APD recordings because of their higher sensitivity to drug-induced APD prolongation and their higher propensity to develop EADs when compared with ventricular muscle (Lu et al., 2002). It is important to emphasize that, for some drugs involved in TdP cases in humans, there is a poor correlation between the hERG IC_{50} values and the results obtained in multi-cellular preparations used for APD recordings (Redfern and Carlsson et al., 2003; Martin et al., 2004). Despite having an IC_{50} in the hERG assay, which would suggest a risk for APD prolongation, some drugs in fact shorten APD or show a bell-shaped dose–response curve on APD (Adamantidis et al., 1993, 1995; Masumiya et al., 2004). The main reason for such discrepancy usually relates to a phenomenon of multiple ion-channel block (lack of selectivity for a given channel target) displayed by such compounds (Delpon et al., 1999). Indeed, in more integrated experimental models involving multi-cellular preparations, the block of inward currents (mainly the fast inward current or the L-type calcium current) may counterbalance the hERG block within the same concentration range and result in APD shortening. Another reason may be different expression levels of several types of ion channels (cell-, tissue-, and species-dependent), which usually lead to conflicting results between laboratories using different methods. For instance, the I_{Ks} component of the delayed rectifier current is expressed at lower levels in dog ventricular myocytes (Lui and Antzelevitch, 1995), rabbit ventricular myocytes (Salata et al., 1996), or human atrial tissue (Li et al., 1996), as compared to guinea pig ventricular myocytes (Sanguinetti and Jurkiewicz, 1991). In the latter species, the presence of a strong I_{Ks} current can mask the APD prolonging effects of I_{Kr} inhibition. Although the choice of the species is still a matter of debate, dogs and rabbits are

generally considered to be the best candidates to assess the risk for humans (Dumotier et al., 1999; Gintant et al., 2001; Lu et al., 2002).

It is important to note that APD recordings from a multi-cellular preparation, such as the PF assay, do not integrate all mechanisms potentially involved in TdP at the whole heart level. Triggered activity may be induced in multi-cellular cardiac preparations, whereas re-entry phenomena cannot be modeled with Purkinje. In addition, stimulation rates used in models that favor EADs and triggered activity in isolated cardiac tissue are generally much lower than the physiologic range. Finally, bursts of sustained triggered activity observed in these preparations generally do not exceed 120 beats per minute, which is sensibly lower than the rate of TDP complexes observed in patients.

1.2.3. Dispersion of repolarization

Despite the evidence that QT interval prolongation (LQTS) is one of the substrates for TdP, the fact that such arrhythmias may also appear in the absence of LQTS radically changed the scientific approach of detecting and considering the underlying mechanisms triggering TdP. Numerous studies demonstrated the role of the ventricular dispersion of repolarization and, more precisely, the role of transmural (Shimizu and Antzelevitch, 1999) intra- and inter-ventricular dispersion (Verduyn et al., 1997a, b) in triggering TdP. Indeed, compounds known to induce TdP in humans have been shown to exacerbate the dispersion of ventricular repolarization. By contrast, some compounds known to induce LQTS with low propensity to induce TdP have been demonstrated to minimally affect ventricular dispersion (Sicouri et al., 1999; Di Diego et al., 2003).

Several models have thus been developed to take into account physiological mechanisms of drug-induced TdP (Carlsson et al., 1990; Hondeghem et al., 2001). Numerous validation studies using different indices of ventricular dispersion reinforced the assumption that prolongation of the repolarization process by itself is not the sole event initiating TdP, and that disproportional heterogeneity of repolarization (spatial and temporal dispersion) is an important factor constituting an ideal substrate for the development of TdP (Habbab and El Sherif, 1990; Antzelevitch, 2004).

This scientific drive for a better understanding of the mechanisms underlying TdP has resulted in the development of experimental models which appear to be more integrative than multi-cellular preparations, such as arterially perfused left ventricular wedge preparations (Di Diego et al., 2003) or isolated whole heart models (Zabel et al., 1997; Eckhard et al., 1998; Gerhardy et al., 1998; Drolet et al., 2003).

Some of these systems use specific pro-arrhythmic indices, such as triangulation of the repolarization phase, APD instability (beat-to-beat variability), reverse use-dependence (Hondeghem and Snyders, 1990) and dispersion of repolarization (Hondeghem et al., 2001). These experimental models have been proven to be reliable methods for the detection of pro-arrhythmic signals in TdP-like arrhythmias.

1.2.4. Electrocardiogram

The ECG represents series of waves generated by electrical events of the different chambers and conduction pathways within the heart. ECG recording in animals helps detect pro-arrhythmic indices based on the analysis of the different waves and helps characterize the nature of the

observed arrhythmias. A general assessment of the risk for drug-induced TdP is mainly based on the ability of the NCE to prolong the QT interval, induce abnormal T wave or U wave, and/or TdP. The QT interval on the ECG is measured from the start of the QRS complex to the end of the T wave. It is difficult to measure the QT interval accurately, due of the lack of precision in determining the exact end of the T wave and when U waves, which tend to merge with the end of the T wave, are present. Additionally, U waves may represent some abnormalities, such as hypokalemia, even though they may also be present in the ECG under normal conditions.

Numerous experimental systems aimed at inducing TdP-like arrhythmias have been developed (Verduyn et al., 1997a, b; Carlsson et al., 1990; Weissenburger et al., 2000). However, such models have serious limitations due to the particular experimental conditions used, e.g., bradycardia induced by AV block, hypokalemia induced by diuretics. These complex protocols again stress the inherent difficulties in inducing TdP experimentally. When they develop, such induced arrhythmias typically do not display the classical TdP morphology; moreover, tachycardia rarely terminates spontaneously, which is different from the clinical situation. QTc increases are thus used as a surrogate marker. Minimum values of QTc increases that are considered significant are usually of the order of 10% in animal species (Hammond et al., 2001), whereas in humans, a relatively modest prolongation of 5 ms is a matter of concern. Indeed, so far, there has not been a single preclinical method, including in vivo animal models, shown to be 100% predictive of the risk for TdP occurrence in humans. In addition, the respective relevance of the animal models (including non-human primates) for such arrhythmias is still a matter of debate. The fact that reproducibility of TdP is not always achievable in animals even in the presence of highly potent I_{Kr} blockers suggests that other predisposing factors or unknown combinations of factors are involved in acquired LQTS-induced TdP.

1.3. Modeling methodologies applicable to safety assessment

This study proposed the use of two types of simulation modeling: forward modeling to predict clinical pro-arrhythmic risk from channel-level pharmacology and reverse modeling to allow estimation of ion-channel pharmacology from canine Purkinje AP traces.

One or more models of markers predictive of pro-arrhythmic risk in patients were required. Surface ECGs are the standard measure used in the clinical assessment of the pro-arrhythmic potential of drugs. At the time of this study, sufficiently predictive computer models of human ECGs were not available; simulations of canine transmural ECG (TxECG) experiments were used instead. This assay is a good experimental analog for the human ECG and can model drug-induced changes in QT interval as well as changes in T-wave morphology that are accepted markers of pro-arrhythmic risk (Yan and Antzelevitch, 1998; Yan et al., 1998; Dumaine et al., 1999; Antzelevitch and Fish, 2001; Zygmunt et al., 2001; Thomas et al., 2003). Recently, computer models of APs in human cardiac myocytes have become available (Ten Tusscher et al., 2004) which may make it possible to simulate human ECGs in future drug studies.

In order to perform the ECG simulations, the effects of each compound on all of the key ion currents were required. These ion-channel-level effects are not generally available in practice. The approach used was to reverse-engineer ion-channel pharmacology from the canine APs. Such an approach requires a *forward* simulation model of the canine PF assay, which measures the time course of transmembrane AP while varying electrical pacing and drug dose according to a

specified protocol. In this study, the ion-channel effects of test drugs were estimated using the Purkinje model and non-linear parameter estimation techniques. The models and non-linear estimation techniques used in this study are reviewed in the following sections.

2. Methods

2.1. Experimental methods

2.1.1. Preparation of guinea pig ventricular myocytes

Single ventricular myocytes were isolated from guinea pigs using a method modified from Salata et al. (1996). Briefly, male guinea pigs (250 g) were killed by cervical dislocation. Thoracotomy was subsequently performed, and the heart was removed and immediately transferred to oxygenated (100% O₂) cold saline. The heart was perfused retrogradely at 10 ml/min through the aorta with an oxygenated Ca²⁺-free saline at 37°C in three stages: first with standard Ca²⁺-free saline for 5 min, second with the same solution containing 280 U/ml type II collagenase (Worthington Biochemical, Lakewood, NJ) plus 0.75 U/ml type XIV protease (Sigma-Aldrich, St. Louis, MO) for 8 min, and finally with saline containing 0.2 mM CaCl₂ for additional 7 min. The left ventricle cut into small pieces was gently shaken at room temperature for about 5 min to disperse single myocytes. The isolated myocytes were then maintained at 37°C for electrophysiological recording, usually within 48 h after isolation.

2.1.2. Patch-clamp measurements for hERG, L-type Ca²⁺ and Na⁺ currents

hERG patch-clamp experiments were performed with HEK293 cells stably transfected with hERG cDNA (C.T. January, University of Wisconsin, USA). Sodium channel patch-clamp experiments were performed with HEK293 cells stably transfected with SCN5A cDNA (S. Heinemann, University of Jena, Germany). Cells were kept under standard cell culture conditions (Traebert et al., 2004).

All ionic currents were recorded using the whole-cell configuration of the patch-clamp technique (Hamill et al., 1981). Electrodes (2–5 MΩ resistance) were made using a DMZ universal puller (Zeitz-Instruments, Munich, Germany) from glass capillary tubes (WPI, Sarasota, FL). For hERG and sodium channel recordings, electrodes were filled with the following solution: KCl 130; MgCl₂ 1.0; ethylene glycol-bis (β-aminoethyl ether)-N,N,N',N'-tetraacetic acid (EGTA) 5; Mg-ATP 5; N-2-hydroxyethylpiperazine-N'-2-ethanesulfonic acid (HEPES) 10; pH 7.2 with 1 M KOH. For Ca²⁺ channel recordings, the electrode solution contained 130 mM cesium methanesulfonate, 20 mM tetraethylammonium chloride, 1 mM MgCl₂, 10 mM EGTA, 10 mM HEPES, 4 mM Tris-ATP, 0.3 mM Tris-GTP, 14 mM phosphocreatine, 50 U/ml creatine phosphokinase, pH 7.2 with CsOH. The external solution for hERG and sodium channel recordings contained the following: NaCl 137; KCl 4; CaCl₂ 1.8; MgCl₂ 1.0; D-glucose 10; HEPES 10; pH 7.4 with 1 M NaOH. The external solution used for recording Ca²⁺ currents contained the following: 137 mM NaCl, 5.4 mM CsCl, 1.8 mM CaCl₂, 1 mM MgCl₂, 10 mM HEPES, 10 mM glucose, pH 7.4 with NaOH. All ionic currents were recorded at 35 ± 1°C using a Heka amplifier (Heka Electronics, Germany). Currents were analyzed using the pulse suite of software (Heka electronics). IC₅₀ values were obtained by sigmoidal fit of the data (SigmaPlot).

For hERG current measurements cells were held at -75 mV, depolarized to $+10$ mV for 500 ms and then repolarized to -40 mV for 500 ms to produce the tail current. Ca^{2+} currents were elicited by a depolarizing step to 0 mV from a holding potential of -40 mV. For the sodium current measurements cells were held at -100 mV and depolarizing pulses to $+20$ mV were delivered. All voltage protocols were delivered at a frequency of 1 Hz as a train of 50 pulses.

2.2. Mathematical modeling methods

2.2.1. Simulation of the canine wedge transmural electrocardiogram

The TxECG model used in this study was developed using the techniques described in Viswanathan et al. (1999) and Viswanathan and Rudy (2000). The model was then adapted to a canine preparation by replacing the Luo-Rudy cell models with commercially developed canine myocyte models based upon work by Rice and others (Jafri et al., 1998; Rice et al., 1998, 1999a, b, 2000). Fig. 1 is a schematic diagram that illustrates the key ion currents represented in the myocyte models. Cellular coupling conductances and key ion-channel current strengths were scaled as a function of wall depth to match the transmural resistivity, AP, and ionic current profiles reported by Antzelevitch and colleagues (Antzelevitch et al., 1999; Shimizu and Antzelevitch, 1998; Yan and Antzelevitch, 1998; Yan et al., 1998). This model also has modifications to account for differences due to sex, history of congestive heart failure, and variations in extracellular electrolytes. These are the major patient risk factors recommended for consideration by the FDA in FDA (2004a, b). Recently, integrative computer models incorporating data from particular genetic variants of ion channels have proven useful in linking altered channel function to the mechanisms of arrhythmia in patients (Clancy and Rudy, 1999, 2001, 2002; Liu et al., 2002, 2003; Clancy et al., 2003). These genetic variations are an additional source of individual patient risk and a promising area of continued investigation, but only results using drug dose and pacing rates as risk factors are presented in this paper.

In order to simulate drug-induced changes to ECG, control simulations of transmembrane APs and TxECG were performed with no drug. The effects of each test compound were then evaluated at concentrations of 0.1, 0.2, 0.5, 1, 2, 5, and $10 \mu\text{M}$. Pacing rate dependence of the test

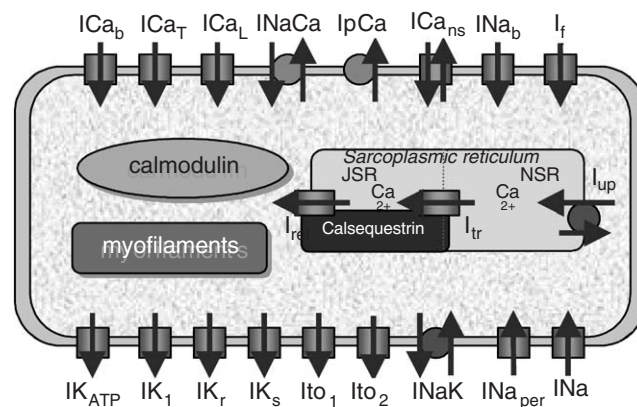


Fig. 1. A schematic representation of transmembrane ion currents responsible for the generation of APs and ECG in the mathematical models used in this study.

compound's actions were evaluated by simulating APs at basic pacing cycle lengths (BCL) of 300, 500, 800, 1000, 2000, and 4000 ms. Following changes in drug concentration or pacing rate, APs were simulated for sufficient time (10 cycles) to allow stabilization before making measurements.

2.2.2. Simulation of drug effects on repolarization

A simple pore-block model was used to account for the effects of drugs. The effects of drugs were modeled using the standard sigmoid dose–response curve parameterized by the half-maximal response dose, IC_{50} . For ion currents (I_x) affected by a test compound, the model assumes that the channel-specific IC_{50} ($IC_{50,x}$) and Hill coefficient (N_x) characterize a sigmoidal dose–response relationship for the inhibition of current (I_x vs. $I_{x,control}$) as a function of concentration, [Drug]. Unless otherwise stated, the Hill coefficient was fixed at $N_x = 1.0$:

$$\frac{I_x([Drug])}{I_{x,control}} = \frac{1}{1 + ([Drug]/IC_{50,x})^{N_x}}.$$

This simple pore-block model was sufficient for these compounds but has been shown to be insufficient to describe the action of many drugs (Starmer et al., 1984; Starmer and Grant, 1985; Irvine, 1998; Irvine and Jafri, 1998; Irvine et al., 1999). All of the improved models proposed in these references are more complex. It is an open question whether the parameters of these complex models will be observable from standard Purkinje AP data.

2.3. Rapid development of a Purkinje fiber model

While rabbit Purkinje models have been published (DiFrancesco and Noble, 1985), no model of the canine Purkinje preparation used in this study was readily available. The simulations of the canine ventricular myocyte (CVM) model were found to be closer than the rabbit Purkinje model to the in vitro behavior of canine PF. This may be due in part to recent developments in calcium handling and other differences between recently published models and DiFrancesco–Noble, and also due to the fact the hyperpolarization activated current, present in the DiFrancesco–Noble model, is not observed in the preparations used for drug safety assessment (Cordeiro et al., 1998; Lu et al., 2002). This initial study led to the hypothesis that one could develop a “rapid prototype” PF model by adjusting the macroscopic conductances of the 14 ion currents represented in the myocyte model.

Non-linear parameter estimation techniques were used to estimate the conductance parameters in the myocyte model to fit the PF data. The conductances were calibrated using APs from samples at multiple pacing rates with no drug and with various doses of a reference compound, *dl*-sotalol. Conductances estimated from calibration data were compared to experimentally observed currents differences published in Cordeiro et al. (1998) and Lu et al. (2002). The results of this validation step are discussed in a later section. The canine Purkinje model thus developed represents a novel model of canine Purkinje; however, it is to be considered a model of the in vitro experiment and not a model of Purkinje under physiological conditions.

2.3.1. Estimation of ion-channel pharmacology from action potential measurements

Given a model of our Purkinje experiments, the next step was to reverse engineer the ion-channel pharmacology of each compound from the laboratory AP data. Since estimates of I_{Kr}

pharmacology were already available from HEK/hERG data, only the other cardiac ion currents ($I_{\text{Na,sus}}$, I_{CaL} , I_{Ks} , I_{to1} , I_{NaCa}) responsible for repolarization were considered in the study. Large variation among preparations in AP morphology, as seen in Fig. 3, if ignored, would have been an important source of error in this analysis. The standard deviation of baseline APD_{90} was approximately 40 ms for all the preparations used to study COMPOUND A. This variation exceeded the change in APD_{90} caused by the compound. Such large variation would have biased estimates of ion-channel pharmacology, so it was necessary to normalize the PF model to each preparation. This was accomplished by estimating the conductance parameters to fit the 0-dose (0.5 and 1.0 Hz) traces for that preparation.

For each drug data set, the parameter estimation step returned five IC_{50} values, corresponding to best fit of each of the five non- I_{Kr} currents. Monte-Carlo analysis was then used to generate minimum and maximum plausible values for each IC_{50} value, defining a range of IC_{50} combinations that well described the AP data. The threshold used to determine the uncertainty range was two-fold over the best score. These confidence intervals were then used to identify significant ion-channel pharmacology. Drug effects on any currents for which the confidence interval contained $\text{IC}_{50} > 100 \mu\text{M}$ were deemed not significant.

2.3.2. Data preprocessing

In all AP fitting activities described in this study, the AP data were truncated to remove the stimulus artifact and the post-repolarization plateau. Each trace was voltage-shifted to match the 0-dose baseline voltage to the baseline voltage predicted by the model. Each AP trace was also time-shifted to synchronize the time of maximum upstroke velocity. In addition to the 14 conductance parameters, a stimulus time offset parameter was used to account for the variable delay between the real stimulus time and the observed AP onset. The delay was due to the spatial separation between the stimulus and recording electrodes in the PF preparation, which was not accounted for in the model.

2.3.3. Optimization

Local optimization (FMINSEARCH from MATLAB) was used for all non-linear parameter estimations. The success of this method proved to be strongly dependent upon the initial parameter estimates, so the results were subsequently checked by global optimization methods (Storn and Price, 1996; Price and Storn, 1997). Bounds constraints held the conductance parameters to be non-negative by assigning a penalty to the error function value to $+\infty$ if any of the parameters were negative. IC_{50} parameters were held strictly positive by performing unconstrained optimization on the $\log_{10}(\text{IC}_{50})$ values.

2.3.4. Error metrics

Time-weighted error metrics were used to compare predicted and measured AP recordings to compensate for the non-uniform sampling rate used in the experiments. For a collection of values $\{f_1, \dots, f_N\}$ at times t_1, \dots, t_N , define $\|\{f_j\}\|^2 \equiv \sum_1^{N-1} (f^2(t_{j+1}) + f^2(t_j))(t_{j+1} - t_j)/2$. (This metric is a discrete approximation to the square of the L_2 -norm of $f(t)$, a function defined continuously on the interval $[t_1, t_N]$.) Given a parameter vector p , a model $y(t;p)$, a predicted AP recording $y_1 = y(t_1;p), \dots, y_N = y(t_N;p)$ and an observed AP recording z_1, \dots, z_N defined at times

t_1, \dots, t_N , we define $E(P)$ to be the *relative* error between predicted and observed AP traces, based on the metric defined above: $E(p) \equiv \|\{y_j - z_j\}\|^2 / \|\{z_j\}\|^2$.

For the CVM to PF conversion step, the 14 conductance values, represented as a vector G , were fitted minimizing the maximum error $E(G)$ over all of available dose and pacing rate combinations. The I_{Kr} IC_{50} for the pure I_{Kr} blocker (*dl*-sotalol) was also allowed to vary but remained within its experimentally determined confidence interval. For the individual PF calibration step, a fit of G was made to the 0-dose AP traces by minimizing the sum over both pacing rates (0.5 and 1.0 Hz) of $E(G)$. For the IC_{50} estimation step, the five unknown IC_{50} values, represented by the vector F , were estimated by minimizing the maximum error $E(F)$ over all of the pacing rate and concentration combinations for which AP data were available.

A number of weighting schemes were tested; all of the metrics described above were found to work well in practice. Subsequent investigations showed that statistically based weighting schemes, e.g., χ^2 , also perform well and have the advantage of a statistical interpretation.

3. Results

3.1. Experimental results

3.1.1. COMPOUND A and COMPOUND B

During preclinical safety assessment, COMPOUND A and COMPOUND B were found to inhibit the maximum hERG tail current with an IC_{50} of 1.48 and 1.82 μM , respectively, in a standard patch-clamp hERG assay performed at 37°C, using hERG stably transfected in HEK293 cells.

Subsequently, additional preclinical results obtained in canine PF stimulated at the rates of 1 and 0.5 Hz in the presence of COMPOUND A and COMPOUND B suggested a mixed ion-channel blocking effect instead of a pure hERG blocking effect. Indeed, instead of a concentration-dependent APD prolonging effect developing at the plateau level and enhanced at lower stimulation rates, the effects of COMPOUND A and COMPOUND B on APs recorded from canine PFs were characterized by an APD shortening starting at the plateau level, which subsequently reduced the duration of the final repolarization phase at both rates (Fig. 2).

The vehicle used was 0.1% DMSO. At the stimulation rate of 1 Hz, the APD measured at 60% of repolarization (APD_{60}) was found to be significantly decreased with COMPOUND A (0.1, 0.3, 1, 3, and 10 μM ; $n = 4$) at the concentrations of 3 ($-19 \pm 6\%$ vs. vehicle) and 10 μM ($-31 \pm 8\%$ vs. vehicle). COMPOUND A significantly decreased APD at 90% of repolarization (APD_{90}) at 3 ($-12 \pm 5\%$ vs. vehicle) and 10 μM ($-18 \pm 6\%$ vs. vehicle) (see Table 1).

At the stimulation rate of 1 Hz, APD_{60} and APD_{90} were not significantly modified by COMPOUND B (0.1, 0.3, 1, 3, and 10 μM ; $n = 6$) at any of the concentrations tested (see Table 1).

In addition to the effects on the repolarization phase, COMPOUND A significantly decreased the AP amplitude (APA) at 1 ($-8 \pm 3\%$ vs. vehicle) and 10 μM ($-15 \pm 5\%$ vs. vehicle). The other parameters (maximum rate of depolarization, MRD; resting membrane potential, RMP) were not altered by increasing concentrations of COMPOUND A. COMPOUND B did not significantly modify APA, upstroke amplitude (UA), and RMP.

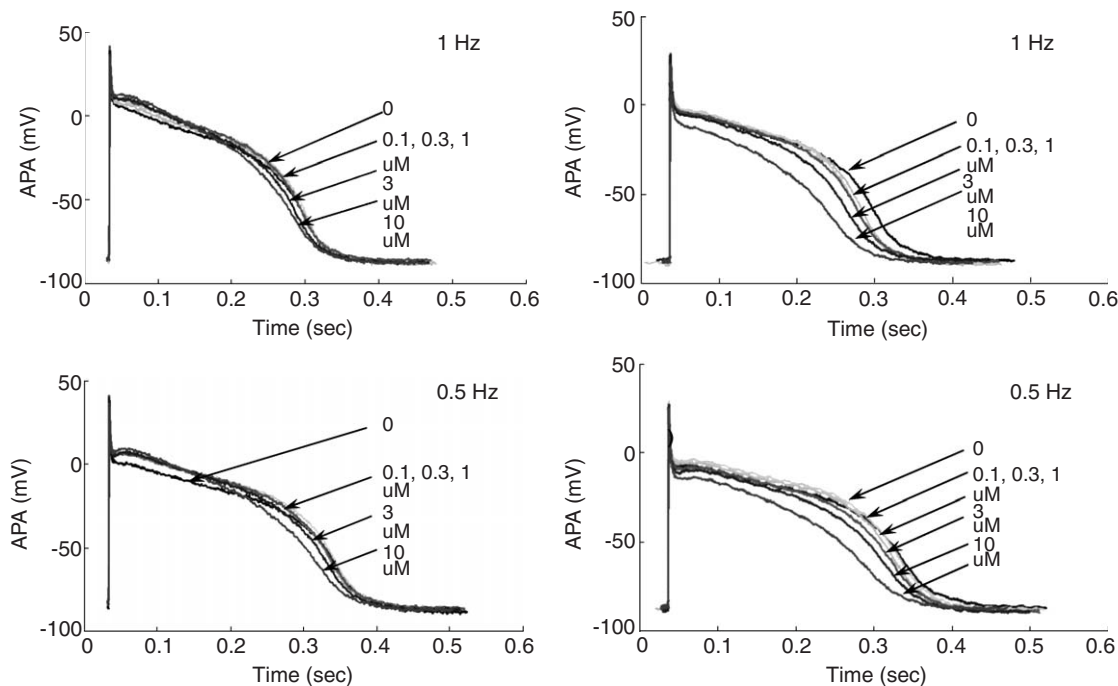


Fig. 2. (Left) Concentration–response relationship of COMPOUND A on the AP in the canine PF preparation paced at 1 and 0.5 Hz. (Right) Concentration–response relationship of COMPOUND B on the AP in the canine PF preparation paced at 1 and 0.5 Hz.

In summary, no APD prolongation (APD_{60} or APD_{90}) in canine PFs was observed in the presence of COMPOUND A or COMPOUND B up to $10 \mu\text{M}$ despite IC_{50} s on hERG in the low micromolar range for both drugs. By contrast, the only statistically significant finding throughout the study was an APD shortening in the presence of high concentrations of COMPOUND A (3 and $10 \mu\text{M}$). This feature strongly suggests that both COMPOUND A and COMPOUND B may reduce other types of ion currents such as the inward L-type calcium current or the sustained inward sodium current, both involved in the maintenance of the plateau phase in PFs. Reducing these currents may have masked the APD prolongation associated with the measured hERG inhibition.

3.1.2. Summary

The preclinical data obtained for COMPOUND A and COMPOUND B showed strong evidence that these drugs may not only block the delayed rectifier potassium current (I_{K_r}), but are also likely to interact with the sodium (I_{Na}) and calcium (I_{CaL}) channels. No previous study at ion-channel level had characterized the compounds' effects on these two channels, as well as on the slowly activating component of the delayed rectifier (I_{K_s}). Reducing I_{K_s} current (loss of function by mutations in the gene encoding for this channel or by pharmacological actions) has been demonstrated to cause QT prolongation without the attendant risk accompanying pure I_{K_r} blockers (Shimizu and Antzelevitch, 1998). Moreover, the SCN5A-mediated cardiac sodium

Table 1
Effects of COMPOUND A, COMPOUND B, and DMSO buffer on action potential parameters

Action potential parameters	Drug A 0.1 μ M	Drug A 0.3 μ M	Drug A 1 μ M	Drug A 3 μ M	Drug A 10 μ M
RMP (mV)	-1.0 ± 0.4	-0.3 ± 0.9	-1.0 ± 1.3	0.1 ± 0.6	-1.1 ± 0.5
UA (mV)	1.4 ± 0.5	0.2 ± 1.4	-2.7 ± 2.9	-3.4 ± 2.7	-9.9 ± 3.6
MRD (%)	3.1 ± 6.4	3.1 ± 4.3	-1.6 ± 4.9	-5.6 ± 8.2	-17.4 ± 18.2
APD ₆₀ (%)	0.9 ± 2.4	4.0 ± 4.6	1.3 ± 3.9	-7.5 ± 2.9	-18.3 ± 7.0
APD ₉₀ (%)	-0.3 ± 2.2	1.0 ± 3.4	-0.7 ± 2.6	-5.0 ± 2.6	-10.4 ± 5.2
	Drug B 0.1 μ M	Drug B 0.3 μ M	Drug B 1 μ M	Drug B 3 μ M	Drug B 10 μ M
RMP (mV)	0.3 ± 0.3	0.6 ± 0.6	-0.7 ± 0.6	0.4 ± 1.2	-0.3 ± 0.9
UA (mV)	1.7 ± 1.1	2.0 ± 1.4	1.5 ± 1.1	1.8 ± 1.6	-1.6 ± 0.4
MRD (%)	-2.9 ± 2.5	-1.8 ± 3.8	-6.4 ± 2.5	-6.7 ± 4.9	-12.7 ± 7.2
APD ₆₀ (%)	1.5 ± 1.1	2.2 ± 0.4	3.5 ± 1.9	0.2 ± 4.1	-5.0 ± 5.2
APD ₉₀ (%)	0.9 ± 0.7	1.9 ± 0.9	3.3 ± 2.0	2.0 ± 3.6	-0.6 ± 4.6
	DMSO 0.1%	DMSO 0.1%	DMSO 0.1%	DMSO 0.1%	DMSO 0.1%
RMP (mV)	-0.4 ± 0.4	0.1 ± 0.2	0.1 ± 0.7	-0.3 ± 0.1	0.1 ± 0.5
UA (mV)	2.4 ± 1.6	0.7 ± 0.9	5.1 ± 1.3	5.1 ± 3.0	5.3 ± 3.2
MRD (%)	-4.7 ± 3.2	-0.2 ± 3.0	-2.0 ± 3.7	-0.2 ± 2.5	0.3 ± 3.5
APD ₆₀ (%)	2.5 ± 1.8	6.4 ± 1.9	8.5 ± 3.1	11.2 ± 4.4	12.5 ± 4.3
APD ₉₀ (%)	1.3 ± 0.7	3.1 ± 1.3	4.7 ± 2.1	6.8 ± 3.2	7.9 ± 3.1

current has been shown to contain a late (also known as sustained or window) component, I_{Nasus} , which remains active throughout the plateau phase and serves to sustain the plateau of the AP, especially in PFs (Attwell et al., 1979; Kunze et al., 1985; Sakakibara et al., 1993). Mutations of the SCN5A sodium channel, which enhance this sustained current, have been shown to be responsible for AP prolongation and delay of repolarization in a variant (LQT3) of the LQTS (Wang et al., 1995; Dumaine et al., 1996). Pharmacologic blockade of this inward current has been shown to shorten the AP and mitigate the prolonging effects of I_{Kr} inhibition (Sicouri et al., 1997a, b). Some sodium channel blockers inhibit the late component of the current more potently (i.e., at lower concentrations) than they do the fast (peak) sodium current (Ono et al., 2000; Nagatomo et al., 2002). Ideally, the effect of drugs on peak and sustained sodium current should be characterized independently; however, a reasonable approximation is to treat a compound's action on both portions of the current identically. The impact of combined channel blockade on the risk of QT prolongation and TdP is not well understood and is likely to be multi-factorial. However, several drugs displaying mixed ion-channel blocking effects, i.e., by reducing at the same concentration range both inward and outward currents, have been demonstrated to be devoid of pro-arrhythmic effects (Sicouri et al., 1997a, b; Benardeau et al., 2000).

The modeling approach was next used to extract best-estimate IC_{50} for all major cardiac ion channels from a detailed analysis of the complete canine PF APs. The resulting dose–response

data obtained by modeling was then used to predict the effects of the compounds on AP and TxECG.

3.2. Modeling results

The pure I_{Kr} blocker (*dl*-sotalol) HEK293 (I_{Kr}) data and PF AP data were used to prototype the canine PF assay system from the CVM model. Next, the data measuring the effects of drug COMPOUND A and COMPOUND B on whole-cell patch-clamped currents in HEK293 cells transfected with hERG cDNA (I_{Kr}), and on APs in isolated canine PFs paced at 1 and 0.5 Hz, were used to reverse engineer the drugs' pharmacological profiles on the key non- I_{Kr} ion currents. The resulting IC_{50} profiles were then used to drive the forward simulation study predicting the effects of COMPOUND A and COMPOUND B on isolated cardiomyocytes, individual myocytes in a transmural wedge preparation, and TxECGs. The results of this simulation-based analysis are detailed below.

3.2.1. Rapid prototyping of a Purkinje fiber model from a canine ventricular myocyte model

The original CVM and fitted canine PF conductance parameters for each of the currents are shown in Table 2. The results are in agreement with certain experimental observations on the differences between currents in CVM and PF in canine. In particular, (Cordeiro et al., 1998) experimentally tested rabbit Purkinje potassium currents and compared the results to ventricular myocytes. In agreement with the experimental observations: the estimated IK1 is much smaller in PF than CVM; I_{Kr} and I_{Ks} are still present but are smaller in PF than in CVM. In contrast to the

Table 2
Model parameter values adjusted in this study and their values before and after the CVM to PF conversion step

Parameter	Units	Function	Endocardial model	Purkinje model
IcaLscale	(au)	Scaling factor for L-type calcium current	1	0.5344
KnaCa	(mA/cm ²)	Scaling factor for sodium–calcium exchanger	1500	512.0174
GKr	(mS/cm ²)	Rapidly activating delayed rectifier channel conductance	0.018	0.0072
GKs	(mS/cm ²)	Slowly activating delayed rectifier potassium channel conductance	3	0.0444
GK1	(mS/cm ²)	Inward rectifier potassium channel conductance	0.75	0.1311
GKp	(mS/cm ²)	Plateau potassium channel conductance	0.00828	0.0139
GbCa	(mS/cm ²)	Background calcium channel conductance	5.00E–05	0.0001
GbNa	(mS/cm ²)	Background sodium channel conductance	0.00141	0.0012
GNa	(mS/cm ²)	Fast inward sodium channel conductance	10	6.86
IpCamax	(mA/cm ²)	Maximum sarcolemmal calcium pump current	0.025	0.0016
GNasus	(mS/cm ²)	Sustained sodium channel conductance	0.02	0.0083
Gto1	(mS/cm ²)	Transient outward potassium channel conductance	0.25	0.1864
Gto2	(mS/cm ²)	Calcium-activated chloride channel conductance	0.03	0.0001
INaKmax	(mA/cm ²)	Maximum sodium–potassium exchange pump current	1	1.0031
offset	(s)	Time offset for the delivery of pacing stimuli	0.05	0.0318

Note: Only the bold-faced currents were subject to pharmacological changes in the IC_{50} estimation step of the study.

experimental observation that the Ca-independent transient outward current is larger in PF than CVM, the fitted I_{to1} for PF was smaller than the original CVM value.

3.2.2. IC_{50} predictions for COMPOUND A and COMPOUND B

The observation that COMPOUND A and COMPOUND B block I_{Kr} (HEK/hERG COMPOUND A $IC_{50} = 1.48 \mu\text{M}$, COMPOUND B $IC_{50} = 1.82 \mu\text{M}$) without prolonging APD in the PF assay suggests that these compounds block multiple ion channels. Using the parameter estimation techniques described in Section 2, the best-fit IC_{50} profiles were estimated for the two compounds. Both COMPOUND A and COMPOUND B were predicted to significantly block the sustained sodium (I_{NaSus}) and the L-type calcium (I_{CaL}) currents; the predicted IC_{50} values for these two currents are given in Table 3. The other three currents (I_{NaCa} , I_{Ks} , I_{to1}) were predicted not to play a significant role in the pharmacology of either compound because the IC_{50} ranges for these currents exceeded the “effectively no-block” threshold of $100 \mu\text{M}$.

As a post-estimation validation activity, the respective hERG peak tail current or inward peak Na^+ and Ca^{2+} currents at the last four pulses (pulse 46–50) of each train were used to determine the inhibitory effects of COMPOUND A and COMPOUND B. The drugs were tested at five increasing concentrations with $n = 4–6$ cell per concentration.

hERG: hERG channel activity in stably transfected HEK293 cells was inhibited depending on the dose by COMPOUND A with an $IC_{50} = 1.48 \mu\text{M}$ and by COMPOUND B with an $IC_{50} = 1.82 \mu\text{M}$. The reference compound E-4031 (100 nM) inhibited hERG channel activity by $98.1 \pm 2.3\%$. The effects of COMPOUND A and COMPOUND B on hERG were known at the outset of the study and were not subject to parameter estimation, so these results serve to validate the experimental hERG results used previously.

Table 3
 IC_{50} estimation, uncertainty analysis, and experimental validation results for COMPOUND A and COMPOUND B

	ICalScale	INaCa	IKs	INaSus	Ito1
COMPOUND A					
Global estimates and range					
Min	0.03	0.01	0.00	0.27	53.70
Best	1.28	11.00	> 100	0.47	> 100
Max	3.32	> 100	> 100	2.62	> 100
Local best	33.40			0.27	
Measured	1.29			2.30*	
COMPOUND B					
Global estimates and range					
Min	0.01	0.07	0.03	0.51	0.00
Best	3.47	> 100	> 100	1.11	0.13
Max	28.80	> 100	> 100	3.13	> 100
Local best	13.24			0.59	
Measured	2.15			4.48*	

Note: IC_{50} values are in micromolar. Measured values for sodium currents (marked with “**”) were for peak sodium current, not necessarily the late component represented by I_{NaSus} in the model. Due to project timing the IC_{50} values obtained using local optimization methods (labeled “local best”) were used for the forward simulations.

Calcium: Calcium channel activity in isolated guinea pig myocytes was inhibited depending on the dose by COMPOUND A with an $IC_{50} = 1.29 \mu\text{M}$ and by COMPOUND B with an $IC_{50} = 2.15 \mu\text{M}$. The positive control nifedepine ($1 \mu\text{M}$) inhibited Ca^{2+} channel currents by $95.0 \pm 3.5\%$ ($n = 3$). These experimentally measured values agree very well with and validate those predicted by our global estimation procedure.

Sodium: Sodium channel activity in isolated guinea pig myocytes was inhibited depending on the dose by COMPOUND A with an $IC_{50} = 2.3 \mu\text{M}$ and by COMPOUND B with an $IC_{50} = 4.48 \mu\text{M}$. The positive control tetrodotoxin ($20 \mu\text{M}$) inhibited Na^{2+} currents by $97.2 \pm 3.2\%$ ($n = 3$). These findings are consistent with our estimated IC_{50} s for these drugs.

The quality of fit of the predicted AP traces from these IC_{50} values can be seen in Fig. 3. These plots illustrate visually how much better the multi-channel blockade profiles explain the data than does the “null hypothesis” of I_{K_r} block only.

Given the cost involved in performing patch-clamp testing for the six key repolarization currents in native myocytes, parameter estimation was used instead to extract best-estimate IC_{50} s for all major cardiac ion channels from the complete set of dose- and rate-dependent canine PF APs. The resulting current-level dose-inhibition estimates were then used to perform compound-specific predictions of the compounds’ effects on myocyte AP and TxECG, which are described in the following section.

3.2.3. Forward predictions of action potentials in isolated myocytes

The canine PF data for COMPOUND A and COMPOUND B suggest that these compounds block multiple ion channels. However, the only direct pharmacological evidence of ion-channel blockade was limited to the hERG channel. For comparison, the “null hypothesis” of a pure I_{K_r} blocker (i.e., no effect on other ion channels) was considered. Such a compound represents a canonical example of a QT prolongation and pro-arrhythmia risk and therefore is a good benchmark for comparison. As described in Section 2, a sigmoidal dose–response curve was used to calculate the individual reductions in I_{K_r} channel conductance for a given concentration within the computer models. Since these data have been shown to represent generic I_{K_r} channel inhibition, the results are given in concentrations relative to the I_{K_r} channel IC_{50} rather than the absolute concentration.

The simulated effects of a pure I_{K_r} blocker on APs of Epi and M cells paced at 1000 ms BCL are shown in Fig. 4 (top). As expected, the AP was prolonged in a concentration-dependent fashion by the I_{K_r} blockade and the amount of AP prolongation (as percent of control) was greater in M cells than in Epi cells. No EADs were observed in any simulated AP. Note the time scale extension (*) to account for severe AP prolongation.

The concentration-dependent effects of COMPOUND A on models of isolated myocytes are considerably different than those of the pure I_{K_r} blocker. Rather than causing uniform and significant prolongation of the AP, the response of the M cells to COMPOUND A was biphasic. At concentrations up to $1 \mu\text{M}$, The M cell AP was shortened while at higher concentrations ($5\text{--}10 \mu\text{M}$), the M cell APD increased (vs. simulations at $0.1\text{--}1.0 \mu\text{M}$ concentrations) though it did exceed drug-free control levels. Such a behavior (initial decrease of APD at low drug concentrations, followed by an increase at higher concentrations) does not match experience gained from experiments, and deserves further investigation. Similar to M cell simulations, the Epi AP is shortened by low doses of COMPOUND A. While high doses ($1\text{--}10 \mu\text{M}$) prolong AP up to

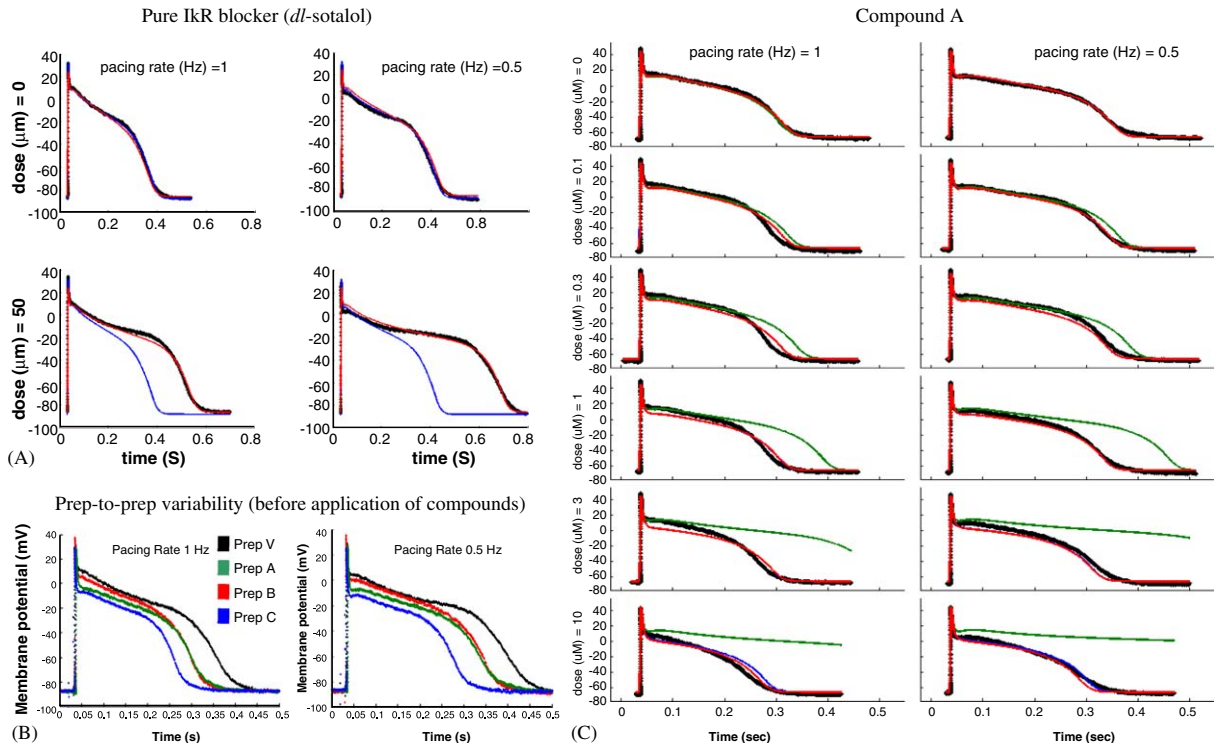


Fig. 3. Validation results for steps in the parameter estimation process. (A) Overlay of fitted PF model predictions to data from APs under control conditions and under the effect of a pure I_{K_r} blocker (*dl*-sotalol). The red curve is the AP prediction from the best-fit parameter set. (B) Comparison of control (0-dose) AP recordings to illustrate the prep-to-prep variability that necessitated calibration of conductance parameters to each pair (0.5 and 1.0 Hz) of AP control traces prior to attempting to fit IC_{50} profiles. “Prep V” refers to the Purkinje preparation used in the Vehicle control pacing studies. “Prep A” and “Prep B” refer to the preparations used to study the effects of COMPOUNDS A and B, respectively. “Prep C” represents an additional preparation, the data from which was not analyzed in this study. (C) Overlay of AP predictions (colored traces) on AP data (black traces) under varying pacing rates and doses of COMPOUND A. The IC_{50} profile corresponding to the “null hypothesis” (COMPOUND A blocks I_{K_r} only) results in APs (green traces) that overshoot the observed data. The red traces are AP predictions from the IC_{50} profile comprised of the known I_{K_r} IC_{50} and the estimated IC_{50} s for I_{Nasus} and I_{CaL} .

levels greater than control, faster pacing rates (500 ms, data not shown) mitigate this behavior. Overall, the absence of AP prolongation in both cell types suggests that the multiple ion-channel blockade of COMPOUND A mitigates the risk of QT prolongation and pro-arrhythmia posed by just the I_{K_r} blocking tendencies.

The concentration-dependent effects of COMPOUND B on models of isolated myocytes are similar to those of COMPOUND A and likewise do not reflect the behavior of a pure I_{K_r} blocker. At all rates, COMPOUND B causes the simulated M cell AP to shorten and the plateau voltage to decrease. Similarly, the Epi AP plateau is diminished with increasing dose, though the APD is largely unaffected until higher concentrations (10 μM at 1000 ms,

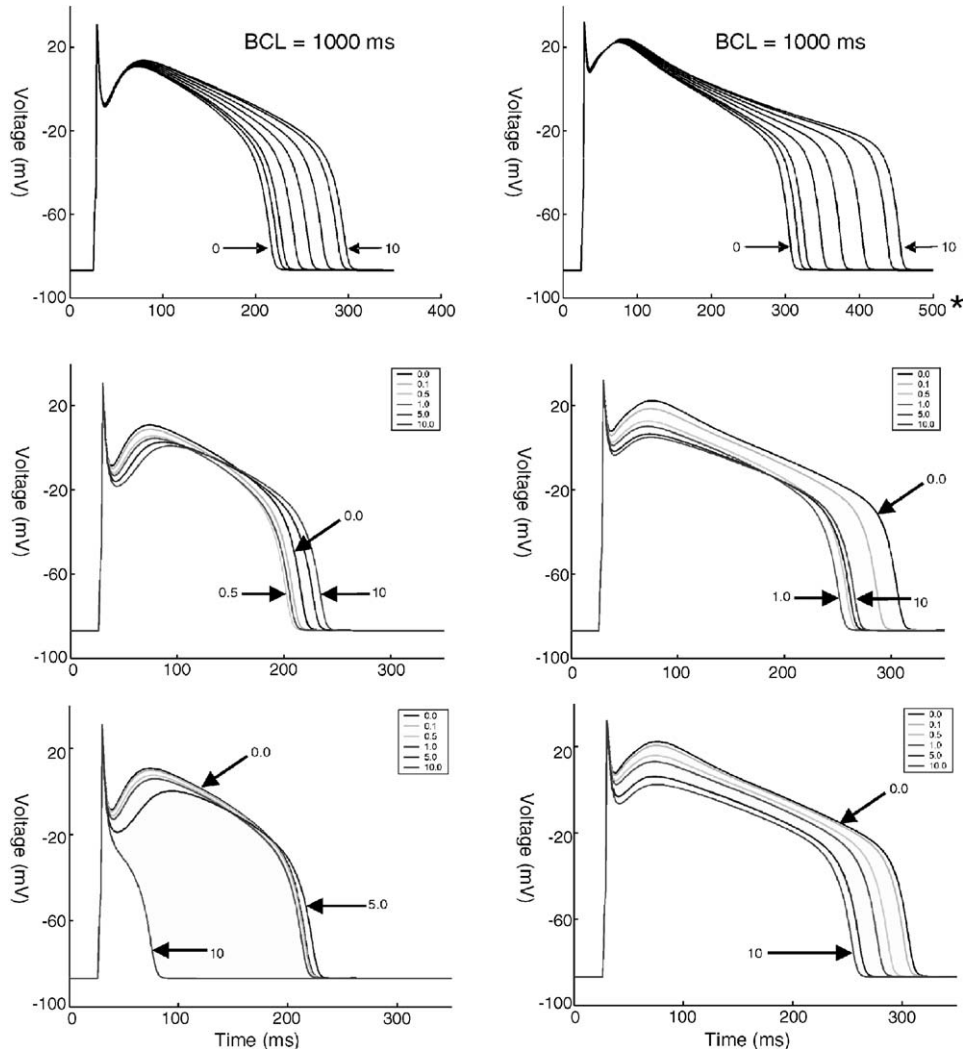


Fig. 4. Concentration-dependent effects of a pure I_{K_r} blocker (top) and COMPOUNDS A (middle) and B (bottom) in computer models of isolated epicardial (Epi) and mid-myocardial (M) cells. Shown are isolated Epi and M cells at BCL 1000ms, under control conditions and for progressively higher concentrations of pure I_{K_r} blocker *dl*-sotalol (0.1 – $10 \times I_{K_r} IC_{50}$), COMPOUND A and COMPOUND B (0.1 – $10 \mu\text{M}$). Heavy arrows indicate the direction of increasing concentration. The asterisk (*) on the time axis indicates the compressed time scale imposed to compensate for severe prolongation seen in this panel.

5 – $10 \mu\text{M}$ at 2000 ms) are reached. At these levels, COMPOUND B has inhibited the calcium influx via L-type channels to the point that calcium-induced calcium release fails to trigger yielding severe AP abbreviation. Because COMPOUND B shortens the M cell AP while leaving the Epi one largely unchanged ($< 5 \mu\text{M}$), the difference in APD shrinks with increasing concentration and suggests that COMPOUND B does not demonstrate significant QT-prolonging capability.

Slow cycle lengths are a known risk factor in the development of drug-induced pro-arrhythmia. When the models were paced at 2000 ms cycle length (data not shown), the behavior for **B** mimicked that observed for 1000 ms pacing; however, the inhibition of calcium influx via L-type channels caused severe shortening of the AP at lower concentrations (COMPOUND A: 10 μ M; COMPOUND B: 5–10 μ M). Rapid pacing at 500 ms cycle length (data not shown) abolished the AP collapse and lessened the drug-induced AP shortening.

3.2.4. Transmural electrocardiogram and dispersion of repolarization

The concentration- and rate-dependent effects of these compounds were also simulated in myocytes embedded in a heterogeneous cable model of the ventricular wall. As observed in isolated cells, increasing concentrations of the pure I_{K_r} blocker in the coupled cable model prolonged the APs of Epi and M cells in a reverse rate-dependent fashion (data not shown). Importantly, electrotonic coupling between the cells modulates the individual cellular response to channel blockade. The extent of AP prolongation in Epi cells was increased (vs. isolated Epi) while the prolongation in M cells was diminished (vs. isolated M). The UA and Phase 1 overshoot in the M cell were also diminished by the electrotonic load of propagation in the cable, a factor absent in isolated cells. The upstroke of the Epi cells did not display the same marked changes because they are located on the cable boundary where the AP terminates and thus do not possess a large electrotonic load for continued propagation.

Analysis of the TxECG computed from the heterogeneous cable model indicates that QT interval is prolonged by a pure I_{K_r} blocker (Fig. 5) in a dose- and reverse rate-dependent fashion though the morphology and orientation of the T wave were unchanged. The concentration- and rate-dependent effects of COMPOUNDS A and B on the key repolarization markers (QT interval, TDR, and APD dispersion) are shown in a more compact form in the first column of Fig. 6. The first pane shows that, for BCL = 1000 ms, the pure I_{K_r} blocker causes significant (10%) QT prolongation at concentrations near $IC_{50}/2$. The next pane in the column shows that increasing I_{K_r} blockade increases the transmural dispersion of repolarization (TDR), measured as the time interval from earliest to latest repolarization across the wall. Increases in TDR have been shown to accompany the substrate for the development of TdP (Antzelevitch et al., 1999; Shimizu and Antzelevitch, 1998, 2000) and therefore may be an alternative to QT prolongation as a marker of true pro-arrhythmic risk. The bottom panel of this figure shows that APD dispersion, measured as the maximum difference in APD across the wall, is increased by slowing the pacing rate and by increasing I_{K_r} blockade.

Like the isolated cell models, the APD of both Epi and M cells in the heterogeneous cable undergo a biphasic response to increasing concentrations of COMPOUND A (data not shown). In both cell types, the minimal APD is reached at the 0.5–1 μ M concentration; however, the extent of prolongation at high doses causes Epi cells to exceed control levels while M cells do not. Thus, APD dispersion is summarily decreased by this drug. The concentration-dependent effect of COMPOUND A on the QT interval measured in the TxECG is likewise biphasic (shortening then lengthening) but alters the T wave morphology substantially (Fig. 5, middle column). Despite the dramatic changes in the T wave, the transmural dispersion of repolarization in the cable is quickly diminished by COMPOUND A (Fig. 6, center). Although there is a moderate increase in TDR as dose is further increased, these values are still below the control values (time interval from earliest to latest cellular repolarization across the wall). The bottom panel shows that APD dispersion,

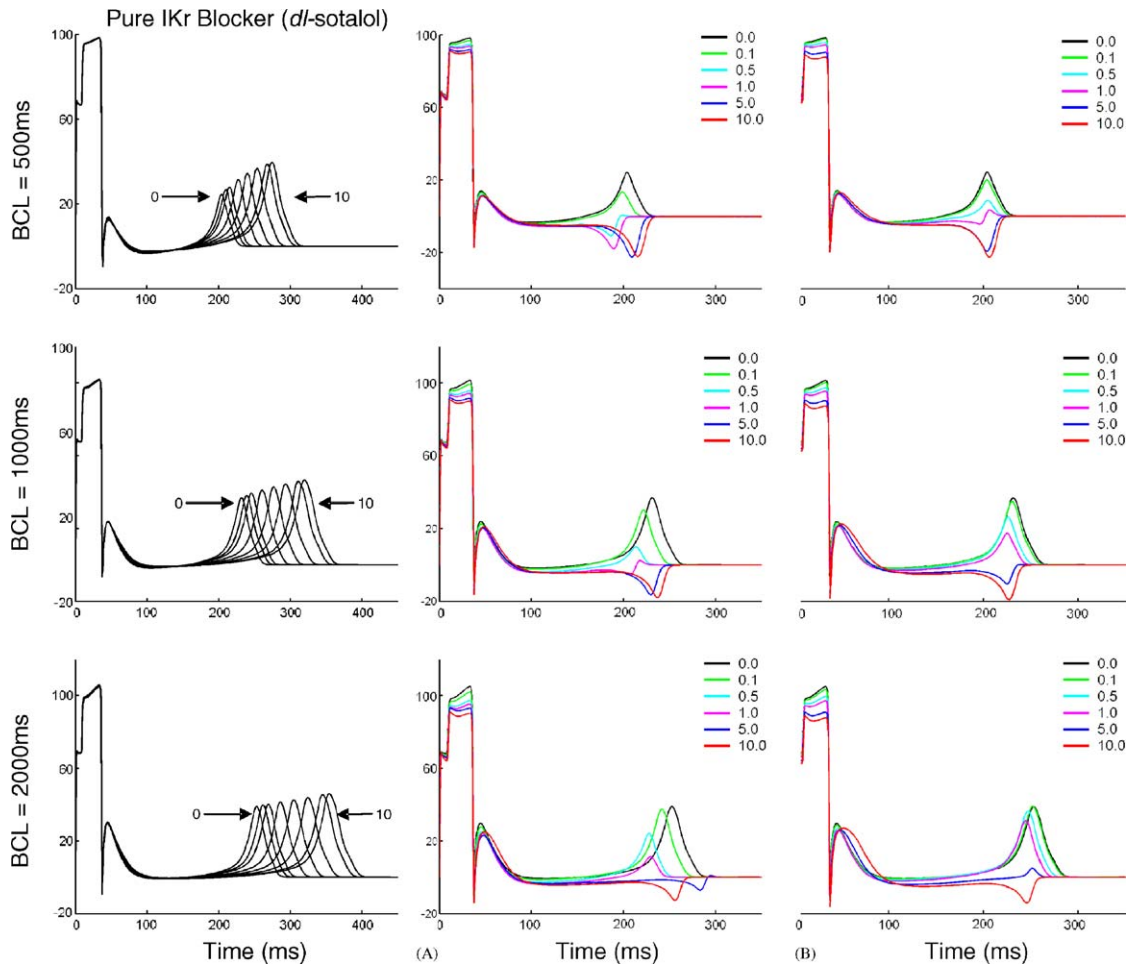


Fig. 5. Concentration- and rate-dependent effects of COMPOUNDS A and B on the TxECG in heterogeneous 1-D cable model of ventricular wall. The results of a pure I_{K_r} blocker are shown for comparison. Shown superimposed are TxECG at BCL of 500, 1000, and 2000ms, under baseline conditions and for progressively higher concentrations (micromolar). For the pure I_{K_r} blocker, concentrations are expressed as multiples of the I_{K_r} IC_{50} .

measured as the maximum difference in APD across the wall, decreases monotonically with the addition of COMPOUND A.

The concentration- and rate-dependent effects of COMPOUND B on TxECG and repolarization markers computed in the spatially heterogeneous cable model are very similar to those of COMPOUND A (Figs. 5 and 6). Like COMPOUND A, TDR, and APD dispersion are diminished by COMPOUND B at all pacing rates. These data taken together suggest COMPOUNDS A and B lack key markers of pro-arrhythmic risk attending a pure I_{K_r} blocker.

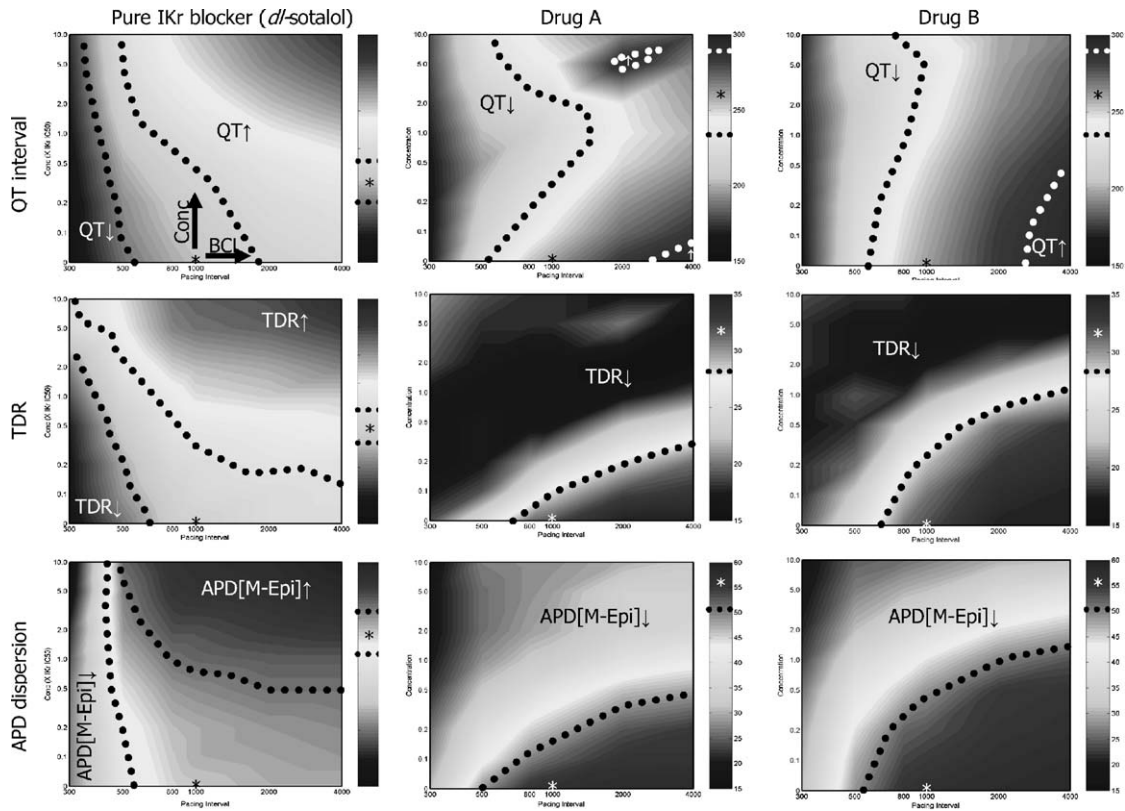


Fig. 6. Concentration- and rate-dependent effects of COMPOUNDS A and B on the QT interval (top row), TDR (middle row), and dispersion of APD (bottom row). The results of a pure I_{K_r} blocker are shown for comparison. Computations were conducted at BCL of 300, 500, 800, 1000, 2000, and 4000 ms, under baseline conditions and for progressively higher concentrations. For the pure I_{K_r} blocker, the concentration ranges from 0.1- to 10-fold of I_{K_r} IC_{50} . For COMPOUNDS A and B the range is (0.1–10 μ M). In each pane, the asterisk indicates the ‘nominal’ parameter set (no drug, pacing rate of 1 Hz). The dotted lines indicate contours at which each safety marker increases or decreases 10% from its nominal value. The colors of the dotted lines, asterisks, and text labels were chosen solely to enhance readability.

4. Discussion

The work presented in this paper represents an important improvement in the practical application of physiologically based mathematical models to the non-clinical cardiac safety assessment process. Previous mathematical modeling efforts produced simulations that can predict the compound effects of cell, tissue, and organ-level cardiac safety markers over many combinations of patient risk factors. Use of these models, however, required characterization of channel-level pharmacology at a level of detail well beyond the industry-standard hERG and PF assays. In this study, the missing data were estimated by applying parameter estimation techniques to hERG and PF assay data.

Parameter estimation techniques were used to prototype a canine PF model from a CVM model by adjusting 14 channel conductance parameters to fit Purkinje AP traces under varying doses of a pure I_{Kr} blocker, *dl*-sotalol. The resulting conductance values provided not only a much-improved fit to the Purkinje data; they also correctly predicted known physiological differences in levels of I_{K1} , I_{Kr} , and I_{Ks} between PFs and myocytes (Cordeiro et al., 1998). The prototype model did not agree with the published differences for I_{to1} , the Ca-independent transient outward current; this discrepancy is a topic of ongoing investigation, but the model was deemed sufficient to proceed to the next step.

The next step in the project was to analyze the AP data from two compounds with known hERG pharmacology and unknown pharmacology on the other cardiac ion currents ($I_{Na,sus}$, I_{CaL} , I_{Ks} , I_{to1} , I_{NaCa}) responsible for repolarization. Our analysis predicted that both compounds cause physiologically significant ($IC_{50} < 100 \mu M$) blockade of $I_{Na,sus}$ and I_{CaL} but not the other three currents. Post-analysis experimental validation studies on these two currents indicate that the predicted IC_{50} values are accurate to within the predicted uncertainty ranges. In order to check the results produced by local optimization, the global optimization technique was used to check the quality and uniqueness of the locally estimated IC_{50} s. The global non-linear optimization technique proved superior to the local estimator, in that it found a better fit to measured APs and the IC_{50} estimates were closer to subsequently measured values, as shown in Table 3.

Finally, the estimated ion-channel pharmacological profiles for the two compounds were used to predict, over many dose and pacing rate combinations, the effects of these compounds on safety markers such as myocyte APD, transmural dispersion of repolarization, and TxECG. The project demonstrated that it is possible to use physiological simulation models to obtain additional decision-making information on the potential risks involved with two preclinical compounds, without requiring non-standard pharmacology assays. This initial success may serve as a template for future integration of simulation modeling into the pharmaceutical non-clinical safety assessment process.

The models and techniques described here have a number of limitations that should be noted. This modeling effort did not fully assess sodium-related conduction disturbances, which may also lead to pro-arrhythmic effects at an integrated tissue level. At the cellular level, the effects of compound-induced sodium current disturbances will need to be assessed in terms of changes in upstroke velocity (V_{max}), UA, and RMP.

The PF model developed in this work represents a novel model, developed by a rapid data-driven prototyping approach that proved successful in the tests described here. Continued development of this computational approach to assess cardiac safety should include: (1) a validation study that examines a library of reference compounds with known mechanism of action on cardiac ion channels, and (2) further development of the PF model to provide a better foundation for the parameter estimation techniques. Future work will likely use the confidence intervals on conductance and IC_{50} values obtained from global estimation to quantify the influence of uncertainty in data on results in the cable model. The number of samples available for this work was too small to estimate sample variability, so future work should characterize this source of uncertainty to improve confidence interval estimates and provide a mechanism for quality control.

The observability of some of the key ion currents, $I_{Na,sus}$, I_{Kr} , and I_{CaL} , from AP data was demonstrated mathematically and experimentally, but others, I_{Ks} , I_{to1} , I_{NaCa} proved less

observable using these techniques (Table 3). This result may be an inherent limitation of the Purkinje assay, as in the case of I_{Ks} , which has little or no effect on Purkinje APs (Cordeiro et al., 1998; Lu et al., 2002), or it may be due to the error metrics chosen. Future work should address this issue, either with additional experimental data or improved analysis methods.

4.1. Toward a simulation-assisted integrated non-clinical safety assessment process

One of the major difficulties in assessing the pro-arrhythmic risk of a pharmaceutical compound is the identification of the rare combinations of drug interactions and patient risk factors that result in increased risk for an otherwise safe drug. It would take hundreds of millions of preclinical experiments and clinical trials with millions of human subjects to analyze what combination of factors promotes an adverse cardiac event, which is not feasible in practice. Another difficulty is that it is not possible to measure directly how the pro-arrhythmic drugs interfere in the normal operation of ion channels in human cardiac cells. Indirect measures, such as changes in patient ECG, are difficult to interpret, due to small sample size, noise in the data and confounding risk factors and drug interactions (FDA, 2003). Therefore, accurately assessing the potential of drug candidates to delay ventricular repolarization leading to a life-threatening arrhythmia should be done as early as possible in preclinical development. Recognizing this need, pharmaceutical regulatory agencies worldwide together with industry and academic scientists have developed the guidance urging the integration of several assays in hopes that their combination will provide a superior measure of true pro-arrhythmic risk (S7B-FDA, 2004). The S7B integrated document does not prescribe a fixed guidance of how to conduct safety pharmacology studies; it contains only two required assays. Hence, each organization chooses its own strategy maximize success during research and development.

The core electrophysiological components of the integrated risk assessment for a given pharmaceutical agent can be divided into *in vitro* and *in vivo* categories (see left panel of Fig. 7). *In vitro* electrophysiology studies employ either single cell experiments (e.g., heterologous expression systems, disaggregated cardiomyocytes) or multi-cellular preparations (e.g., PF; papillary muscle; trabeculae; perfused myocardium; intact heart). Heterologous expression systems, where human ion-channel protein(s) are expressed in non-cardiac cell lines, are used to assess the effects of a compound on a specific ion channel. It needs to be noted that, typically, the ion channel is I_{Kr} . Disaggregated cells and multi-cellular tissue preparations can be useful systems in which to study the effects of compounds on the APD, the AP morphology, and the associated ion currents. While these preparations can facilitate improved understanding of QT-prolonging mechanisms, they are far from ideal since *in vivo* modulators such as plasma protein binding, hormonal regulation, autonomic nervous activity, metabolic clearance, tissue accumulation, and mechanical loading of the ventricular tissue are not taken into consideration. In addition, the spatial heterogeneity of cardiac tissue makes the assessment of any specific cell type somewhat limited in nature.

In vivo animal models allow investigation of electrocardiographic changes, disturbances to repolarization, and associated arrhythmias where integrated effects on the full complement of ion channel and cell types are assessed. Importantly, all of the potential modulators absent from the *in vitro* studies are present in the whole animal; however, these factors can make the interpretation of the assay difficult. However, these experiments are performed in controlled environment with a

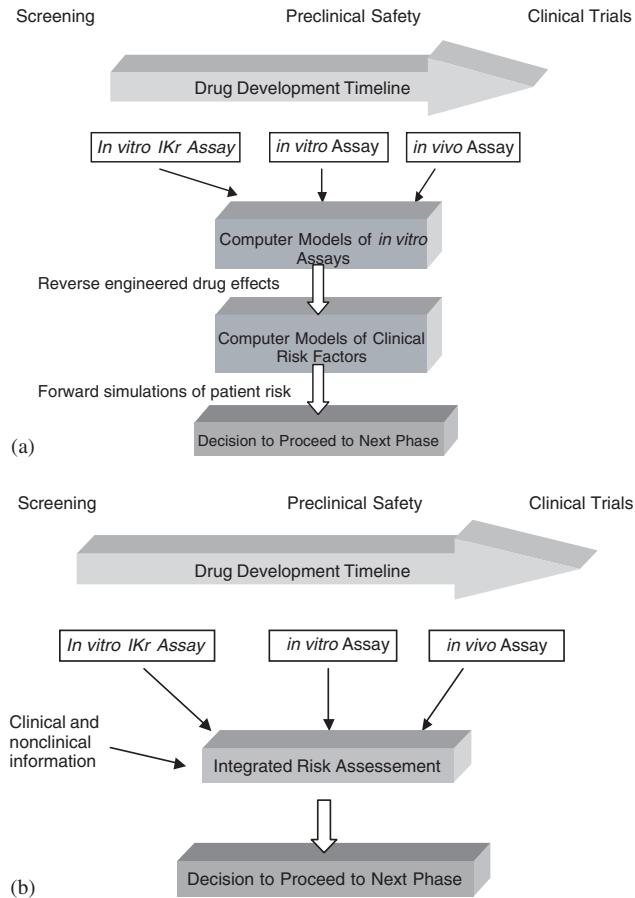


Fig. 7. Experimental assays at different stages of drug discovery and development. (a) At each stage, the new information is added to previous knowledge and used to make incremental decisions whether to continue compound development. (b) Computer models of *in vitro* assays and machine learning algorithms are used to reverse engineer the effects of candidate compounds. The reverse-engineered drug effects are used in forward simulation models to provide an integrated assessment of patient risk.

homogeneous animal population and therefore cannot fully address the risk factors in the clinical situation.

In our proposed process, mathematical modeling provides a mechanistic framework for understanding interactions in an integrative fashion and bridge experimental results that otherwise may seem contradictory, as well as for quantitative risk assessment (see right panel of Fig. 7).

(1) *Simulation models of in vitro assays*: This component requires detailed simulation models that correctly map multiple ion-channel pharmacology of a drug to accurate simulation of the measurements taken in the *in vitro* assay. In this study, a model of canine PF drug safety assay was used. This assay measures the time course of transmembrane APs whilst varying pacing

rates and drug doses. Such models are described by non-linear systems of time-dependent ordinary differential equations (Muzikant and Penland, 2002).

- (2) *Non-linear parameter estimation techniques*: Since detailed ion-channel pharmacology of a drug is rarely known in practice, this component is used to fill gaps in our knowledge by reverse-engineering ion-channel drug effects from the in vitro assay data. The parameter estimation step seeks to find the effect of the drug on each of the eight key ion channels to minimize the error between simulated experiment results and actual data.
- (3) *Simulation of clinical risk factors*: As discussed earlier, the hERG assay and the canine PF measurements are preclinical surrogates for live animal and human tests. This component requires use of simulations of markers of clinical risk. These markers can be clinical measurements, such as human ECG changes, or can be other preclinical measurements, such as canine wedge preparation ECGs, live canine or primate ECG changes. These computer simulations can incorporate models of effects that are not directly tested in the hERG or Purkinje assays, such as patient risk factors, drug–drug interactions, and plasma protein binding of the drug.

The forward clinical risk simulations, calibrated to a particular drug, allow for the possibility to simulate many more experiments, over a wider range of conditions, than are feasible in the laboratory or the clinic. The combination of methods provides a more realistic view of physiological changes due to healthy responses, diseases and therapies, potentially resulting in safer drugs at a lower cost in dollars, animal testing, and human life.

Editor's note

Please see also related communications in this volume by Ward et al. (2005) and Judé et al. (2005). For further downloadable content please see <http://www.physiome.org.nz/publications/pbmb-2005-89/Bottino/>

References

- Abbott, G.W., Sesti, F., Splawski, I., Buck, M.E., Lehmann, M.H., Timothy, K.W., Keating, M.T., Goldstein, S.A.N., 1999. MiRP1 forms I_{Kr} potassium channels with hERG and is associated with cardiac arrhythmia. *Cell* 97, 175–187.
- Adamantidis, M.M., Kerram, P., Caron, J.F., Dupuis, B.A., 1993. Droperidol exerts dual effects on repolarization and induces early afterdepolarizations and triggered activity in rabbit Purkinje fibers. *J. Pharmacol. Exp. Ther.* 266, 884–893.
- Adamantidis, M.M., Lacroix, D.L., Caron, J.F., Dupuis, B.A., 1995. Electrophysiological effects of the histamine Type-1 receptor antagonist astemizole on rabbit Purkinje fibers: clinical relevance. *J. Cardiovasc. Pharmacol.* 26, 319–327.
- Antzelevitch, C., 2004. Arrhythmogenic mechanisms of QT prolonging drugs: is QT prolongation really the problem? *J. Electrocardiol.* 37 (Suppl.), 15–24.
- Antzelevitch, C., Fish, J., 2001. Electrical heterogeneity within the ventricular wall. *Basic Res. Cardiol.* 96 (6), 517–527.
- Antzelevitch, C., Shimizu, W., Yan, G.X., Sicouri, S., Weissenburger, J., Nesterenko, V.V., Burashnikov, A., Di Diego, J., Saffitz, J., Thomas, G.P., 1999. The M cell: its contribution to the ECG and to normal and abnormal electrical function of the heart. *J. Cardiovasc. Electrophysiol.* 10 (8), 1124–1152.

- Attwell, D., Cohen, I., Eisner, D., Ohba, M., Ojeda, C., 1979. The steady state TTX-sensitive (“window”) sodium current in cardiac Purkinje fibres. *Pflügers Arch.* 379 (2), 137–142.
- Carlsson, L., Almgren, O., Duker, G., 1990. QTU-prolongation and torsades de pointes induced by putative class III antiarrhythmic agents in the rabbit: etiology and interventions. *J. Cardiovasc. Pharmacol.* 16, 276–285.
- Clancy, C.E., Rudy, Y., 1999. Linking a genetic defect to its cellular phenotype in a cardiac arrhythmia. *Nature* 400 (6744), 566–569.
- Clancy, C.E., Rudy, Y., 2001. Cellular consequences of HERG mutations in the long QT syndrome: precursors to sudden cardiac death. *Cardiovasc. Res.* 50 (2), 301–313.
- Clancy, C.E., Rudy, Y., 2002. Na⁺ channel mutation that causes both Brugada and long-QT syndrome phenotypes: a simulation study of mechanism. *Circulation* 105 (10), 1208–1213.
- Clancy, C.E., Tateyama, M., et al., 2003. Non-equilibrium gating in cardiac Na⁺ channels: an original mechanism of arrhythmia. *Circulation* 107 (17), 2233–2237.
- Cordeiro, J.M., Spitzer, K.W., et al., 1998. Repolarizing K⁺ currents in rabbit heart Purkinje cells. *J. Physiol.* 508 (Part 3), 811–823.
- Curran, M.E., Splawski, I., Timothy, K.W., Vincent, G.M., Green, E.D., Keating, M.T., 1995. A molecular basis for cardiac arrhythmia: *hERG* mutations cause long QT syndrome. *Cell* 80, 795–803.
- Curtis, L.H., Ostbye, T., et al., 2003. Prescription of QT-prolonging drugs in a cohort of about 5 million outpatients. *Am. J. Med.* 114 (2), 135–141.
- Davidenko, J.M., Cohen, L., Goodrow, R., Antzelevitch, C., 1989. Quinidine-induced action potential prolongation, early afterdepolarizations, and triggered activity in canine Purkinje fibers. Effects of stimulation rate, potassium, and magnesium. *Circulation* 79, 674–686.
- Delpon, E., Valenzuela, C., Tamargo, J., 1999. Blockade of cardiac potassium and other channels by antihistamines. *Drug Saf.* 21 (Suppl. 1), 11–18.
- DiFrancesco, D., Noble, D., 1985. A model of cardiac electrical activity incorporating ionic pumps and concentration changes. *Philos. Trans. R. Soc. London: B Biol. Sci.* 307 (1133), 353–398.
- Drolet, B., Yang, T., Daleau, P., Roden, D.M., Turgeon, J., 2003. Risperidone prolongs cardiac repolarization by blocking the rapid component of the delayed rectifier potassium current. *J. Cardiovasc. Pharmacol.* 41, 934–937.
- Dumaine, R., Towbin, J.A., et al., 1999. Ionic mechanisms responsible for the electrocardiographic phenotype of the Brugada syndrome are temperature dependent. *Circ. Res.* 85 (9), 803–809.
- Dumaine, R., Wang, Q., Keating, M.T., Hartmann, H.A., Schwartz, P.J., Brown, A.M., Kirsch, G.E., 1996. Multiple mechanisms of Na⁺ channel-linked long-QT syndrome. *Circ. Res.* 78, 916–924.
- Dumotier, B.M., Adamantidis, M.M., Puisieux, F.L., Bastide, M.M., Dupuis, B.A., 1999. Repercussions of pharmacologic reduction in ionic currents on action potential configuration in rabbit Purkinje fibers: are they indicative of proarrhythmic potential? *Drug Dev. Res.* 47, 63–76.
- El-Sherif, N., Chinushi, M., Caref, E.B., Restivo, M., 1997. Electrophysiological mechanism of the characteristics electrocardiographic morphology of Torsade de pointes tachyarrhythmias in the long-QT syndrome. Detailed analysis of ventricular tridimensional activation patterns. *Circulation* 96, 4392–4409.
- FDA, 2003. Meeting of the Anesthetic & Life Support Drugs Advisory Committee. FDA, Food and Drug Administration Center for Drug Evaluation and Research.
- FDA, 2004a. Challenge and Opportunity on the Critical Path to New Medical Products. US Food and Drug Administration.
- FDA, 2004b. The Clinical Evaluation of QT/QTc Interval Prolongation and Proarrhythmic Potential for Non Antiarrhythmic Drugs. US Food and Drug Administration, Center for Drug Evaluation and Research.
- Gerhardy, A., Scholtysik, G., Schaad, A., Haltiner, R., Hess, T., 1998. Generating and influencing Torsades de Pointes—like polymorphic ventricular tachycardia in isolated guinea pig hearts. *Basic Res. Cardiol.* 93 (4), 285–294.
- Gintant, G.A., Limberis, J.T., McDermott, J.S., Wegner, C.D., Cox, B.F., 2001. The canine Purkinje fiber: an in vitro model system for acquired long QT syndrome and drug-induced arrhythmogenesis. *J. Cardiovasc. Pharmacol.* 37 (5), 607–618.
- Hammond, T.G., Carlsson, L., Davis, A.S., Lynch, W.G., MacKenzie, I., Redfern, W.S., Sullivan, A.T., Camm, A.J., 2001. Methods of collecting and evaluating non-clinical cardiac electrophysiology data in the pharmaceutical industry: results from an internal survey. *Cardiovasc. Res.* 49, 741–750.

- Hondeghem, L.M., Snyders, D.J., 1990. Class III antiarrhythmic agents have a lot of potential but a long way to go. Reduced effectiveness and dangers of reverse use dependence. *Circulation* 81, 686–690.
- Hondeghem, L.M., Carlsson, L., Duker, G., 2001. Instability and triangulation of the action potential predict serious proarrhythmia, but action potential duration prolongation is antiarrhythmic. *Circulation* 103, 2004–2013.
- Irvine, L.A., 1998. Models of the Cardiac Sodium Channel and the Action of Lidocaine. Johns Hopkins University, Baltimore.
- Irvine, L.A., Jafri, M.S., et al., 1998. A quantitative study of modulated receptor and allosteric effector models of drug action.
- Irvine, L.A., Jafri, M.S., et al., 1999. Cardiac sodium channel Markov model with temperature dependence and recovery from inactivation. *Biophys. J.* 76 (4), 1868–1885.
- Jafri, M.S., Rice, J.J., et al., 1998. Cardiac Ca^{2+} dynamics: the roles of ryanodine receptor adaptation and sarcoplasmic reticulum load. *Biophys. J.* 74 (3), 1149–1168.
- January, C.T., Moccucci, A., 1992. Cellular mechanisms of early afterdepolarizations. *Ann. N.Y. Acad. Sci.* 644, 23–32.
- January, C.T., Riddle, J.M., 1989. Early afterdepolarizations: mechanism of induction and block. *Circ. Res.* 64, 977–990.
- January, C.T., Shorofsky, S., 1990. Early afterdepolarizations: newer insights into cellular mechanisms. *J. Cardiovasc. Electrophysiol.* 1, 161–169.
- January, C.T., Chau, V., Makielski, J.C., 1991. Triggered activity in the heart: cellular mechanisms of early afterdepolarizations. *Eur. Heart J.* 12, 4–9.
- Judé, S., Roger, S., Martel, E., et al., 2005. Dietary long-chain omega-3 fatty acids of marine origin: a comparison of their protective effects on coronary heart disease and breast cancers. *Prog. Biophys. Mol. Biol.* 89.
- Kamiya, K., Mitcheson, J.S., Yasui, K., Kodama, I., Sanguinetti, M.C., 2001. Open channel block of HERG K(+) channels by vesnarinone. *Mol. Pharmacol.* 60 (2), 244–253.
- Kunze, D.L., Lacerda, A.E., Wilson, D.L., Brown, A.M., 1985. Cardiac Na currents and the inactivating, reopening, and waiting properties of single cardiac Na channels. *J. Gen. Physiol.* 86 (5), 691–719.
- Li, G.R., Feng, J., Yue, L., Carrier, M., Nattel, S., 1996. Evidence for two components of delayed rectifier K^+ current in human ventricular myocytes. *Circ. Res.* 78, 689–696.
- Liu, H., Tateyama, M., et al., 2002. Channel openings are necessary but not sufficient for use-dependent block of cardiac Na^+ channels by flecainide: evidence from the analysis of disease-linked mutations. *J. Gen. Physiol.* 120 (1), 39–51.
- Liu, H., Clancy, C., et al., 2003. Mutations in cardiac sodium channels: clinical implications. *Am. J. Pharmacogenomics* 3 (3), 173–179.
- Lu, H.R., Vlamincx, E., Van Ammel, K., De Clerck, F., 2002. Drug-induced long QT in isolated rabbit Purkinje fibers: importance of action potential duration, triangulation and early after depolarization. *Eur. J. Pharmacol.* 452, 183–192.
- Lui, D.W., Antzelevitch, C., 1995. Characteristics of the delayed rectifier current ($I(\text{Kr})$ and $I(\text{Ks})$) in canine ventricular epicardial, midmyocardial, and endocardial myocytes: a weaker $I(\text{Ks})$ contributes to the longer action potential of the M cell. *Circ. Res.* 76, 351–365.
- Martin, R.L., McDermott, J.S., Salmen, H.J., Palmatier, J., Cox, B.F., Gintant, G.A., 2004. The utility of hERG and repolarization assays in evaluating delayed cardiac repolarization: influence of multi-channel block. *J. Cardiovasc. Pharmacol.* 43 (3), 369–379.
- Masumiya, H., Saito, M., Matsuda, T., Noguchi, K., Iida-Tanaka, N., Shigenobu, K., 2004. Lack of prolonging effect of terfenadine on rabbit myocardial tissue preparations. *Biol. Pharm. Bull.* 27, 131–135.
- Muzikant, A.L., Penland, R.C., 2002. Models for profiling the potential QT prolongation risk of drugs. *Curr. Opin. Drug Discov. Dev.* 5 (1), 127–135.
- Nagatomo, T., January, C.T., Ye, B., Abe, H., Nakashima, Y., Makielski, J.C., 2002. Rate-dependent QT shortening mechanism for the LQT3 deltaKPQ mutant. *Cardiovasc. Res.* 54 (3), 624–629.
- Ono, K., Kaku, T., Makita, N., Kitabatake, A., Arita, M., 2000. Selective block of late currents in the DeltaKPQ Na^+ channel mutant by pilsicainide and lidocaine with distinct mechanisms. *Mol. Pharmacol.* 57 (2), 392–400.
- Price, K., Storn, R., 1997. Differential evolution. *Dr. Dobb's J.*, 18–24.

- Puisieux, F.L., Adamantidis, M.M., Dumotier, B.M., Dupuis, B.A., 1996. Cisapride-induced prolongation of cardiac action potential and early afterdepolarizations in rabbit Purkinje fibers. *Br. J. Pharmacol.* 117, 1377–1379.
- Redfern, W.S., Carlsson, L., et al., 2003. Relationships between preclinical cardiac electrophysiology, clinical QT interval prolongation and torsade de pointes for a broad range of drugs: evidence for a provisional safety margin in drug development. *Cardiovasc. Res.* 58 (1), 32–45.
- Rice, J.J., Jafri, M.S., et al., 1998. Modeling short-term interval-force relations in cardiac muscle. *Ann. N.Y. Acad. Sci.* 853, 345–349.
- Rice, J.J., Jafri, M.S., et al., 1999a. Modeling gain and gradedness of Ca^{2+} release in the functional unit of the cardiac diadic space. *Biophys. J.* 77 (4), 1871–1884.
- Rice, J.J., Winslow, R.L., et al., 1999b. Comparison of putative cooperative mechanisms in cardiac muscle: length dependence and dynamic responses. *Am. J. Physiol.* 276 (5 Part 2), H1734–H1754.
- Rice, J.J., Jafri, M.S., et al., 2000. Modeling short-term interval-force relations in cardiac muscle. *Am. J. Physiol. Heart Circ. Physiol.* 278 (3), H913–H931.
- Roden, D.M., 1993. Early afterdepolarizations and Torsades de pointes: implications for the control of cardiac arrhythmias by prolonging repolarization. *Eur. Heart J.* 14, H56–H61.
- S7B-FDA, 2004. ICH S7B Guidelines: The Nonclinical Evaluation of the Potential for Delayed Ventricular Repolarization (QT Interval Prolongation) by Human Pharmaceuticals.
- Sakakibara, Y., Furukawa, T., Singer, D.H., Jia, H., Backer, C.L., Arentzen, C.E., Wasserstrom, J.A., 1993. Sodium current in isolated human ventricular myocytes. *Am. J. Physiol.* 265 (4 Part 2), H1301–H1309.
- Salata, J.J., Jurkiewicz, N.K., Jow, B., Folander, K., Guinasso Jr., P.J., Raynor, B., Swanson, R., Fermini, B., 1996. I_{K} of rabbit ventricle is composed of two currents: evidence for I_{Ks} . *Am. J. Physiol.* 271, H2477–H2489.
- Sanguinetti, M.C., Jurkiewicz, N.K., 1991. Delayed rectifier outward K^{+} current is composed of two currents in guinea pig atrial cells. *Am. J. Physiol.* 260, H393–H399.
- Sanguinetti, M.C., Jiang, C., Curran, M.E., Keating, M.T., 1995a. A mechanistic link between an inherited and an acquired cardiac arrhythmia: *hERG* encodes the I_{Kr} potassium channel. *Cell* 81, 299–307.
- Sanguinetti, M.C., Jiang, C., Curran, M.E., Keating, M.T., 1995b. A mechanistic link between an inherited and an acquired cardiac arrhythmia: *hERG* encodes the $I(\text{Kr})$ potassium channel. *Cell* 81, 299–307.
- Scherer, C.R., Lerche, C., Decher, N., Dennis, A.T., Maier, P., Ficker, E., Busch, A.E., Wollnik, B., Steinmeyer, K., 2002. The antihistamine fexofenadine does not affect $I(\text{Kr})$ currents in a case report of drug-induced cardiac arrhythmia. *Br. J. Pharmacol.* 37 (6), 892–900.
- Shimizu, W., Antzelevitch, C., 1998. Cellular basis for the ECG features of the LQT1 form of the long-QT syndrome: effects of beta-adrenergic agonists and antagonists and sodium channel blockers on transmural dispersion of repolarization and torsade de pointes. *Circulation* 98 (21), 2314–2322.
- Shimizu, W., Antzelevitch, C., 1999. Cellular basis for long QT, transmural dispersion of repolarization, and torsade de pointes in the long QT syndrome. *J. Electrocardiol.* 32 (Suppl.), 177–184.
- Shimizu, W., Antzelevitch, C., 2000. Differential effects of beta-adrenergic agonists and antagonists in LQT1, LQT2 and LQT3 models of the long QT syndrome. *J. Am. Coll. Cardiol.* 35 (3), 778–786.
- Sicouri, S., Antzelevitch, D., Heilmann, C., Antzelevitch, C., 1997a. Effects of sodium channel block with mexiletine to reverse action potential prolongation in in vitro models of the long term QT syndrome. *J. Cardiovasc. Electrophysiol.* 8 (11), 1280–1290.
- Sicouri, S., Moro, S., Litovsky, S., Elizari, M.V., Antzelevitch, C., 1997b. Chronic amiodarone reduces transmural dispersion of repolarization in the canine heart. *J. Cardiovasc. Electrophysiol.* 8 (11), 1269–1279.
- Starmer, C.F., Grant, A.O., 1985. Phasic ion channel blockade. A kinetic model and parameter estimation procedure. *Mol. Pharmacol.* 28 (4), 348–356.
- Starmer, C.F., Grant, A.O., et al., 1984. Mechanisms of use-dependent block of sodium channels in excitable membranes by local anesthetics. *Biophys. J.* 46 (1), 15–27.
- Storn, R., Price, K., 1996. Minimizing the real functions of the ICEC '96 contest by differential evolution. *Evolutionary computation*, 1996. In: Proceedings of the IEEE International Conference on.
- Ten Tusscher, K.H., Noble, D., et al., 2004. A model for human ventricular tissue. *Am. J. Physiol. Heart Circ. Physiol.* 286 (4), H1573–H1589.

- Thomas, G.P., Gerlach, U., et al., 2003. HMR 1556, a potent and selective blocker of slowly activating delayed rectifier potassium current. *J. Cardiovasc. Pharmacol.* 41 (1), 140–147.
- Tristani-Firouzi, M., Chen, J., Mitcheson, J.S., Sanguinetti, M.C., 2001. Molecular biology of K(+) channels and their role in cardiac arrhythmias. *Am. J. Med.* 110, 50–59.
- Verduyn, S.C., Vos, M.A., van der Zande, J., Kulcsar, A., Wellens, H.J., 1997a. Further observations to elucidate the role of interventricular dispersion of repolarization and early afterdepolarizations in the genesis of acquired torsade de pointes arrhythmias: a comparison between almokalant and D-sotalol using the dog as its own control. *J. Am. Coll. Cardiol.* 30, 1575–1584.
- Verduyn, S.C., Vos, M.A., van der Zande, J., van der Hulst, F.F., Wellens, H.J., 1997b. Role of interventricular dispersion of repolarization in acquired Torsade-de-pointes arrhythmias: reversal by magnesium. *Cardiovasc. Res.* 34, 453–463.
- Viswanathan, P.C., Rudy, Y., 2000. Cellular arrhythmogenic effects of congenital and acquired long-QT syndrome in the heterogeneous myocardium. *Circulation* 101 (10), 1192–1198.
- Viswanathan, P.C., Shaw, R.M., et al., 1999. Effects of I_{Kr} and I_{Ks} heterogeneity on action potential duration and its rate dependence: a simulation study. *Circulation* 99 (18), 2466–2474.
- Wang, Q., Shen, J., Splawski, I., Atkinson, D., Li, Z., Robinson, J.L., Moss, A.J., Towbin, J.A., Keating, M.T., 1995. SCN5A mutations associated with an inherited cardiac arrhythmia, long QT syndrome. *Cell* 80, 805–811.
- Ward, C.A., Bazzazi, H., Clark, R.B., Nygren, A., Giles, W.R., 2005. Actions of emigrated neutrophils on Na^+ and K^+ currents in rat ventricular myocytes. *Prog. Biophys. Mol. Biol.* 89.
- Weerapura, M., Nattel, S., Chartier, D., Caballero, R., Hebert, T.E., 2002. A comparison of currents carried by HERG, with and without coexpression of MiRP1, and the native rapid delayed rectifier current. Is MiRP1 the missing link? *J. Physiol.* 540 (Part 1), 15–27.
- Weissenburger, J., Nesterenko, V.V., Antzelevitch, C., 2000. Transmural heterogeneity of ventricular repolarization under baseline and long QT conditions in the canine heart in vivo: torsades de pointes develops with halothane but not pentobarbital anesthesia. *J. Cardiovasc. Electrophysiol.* 11 (3), 290–304.
- Yan, G.X., Antzelevitch, C., 1998. Cellular basis for the normal T wave and the electrocardiographic manifestations of the long-QT syndrome. *Circulation* 98 (18), 1928–1936.
- Yan, G.X., Shimizu, W., et al., 1998. Characteristics and distribution of M cells in arterially perfused canine left ventricular wedge preparations. *Circulation* 98 (18), 1921–1927.
- Yan, G.-X., Wu, Y., Liu, T., Wang, J., Marinchak, R.A., Kowey, P.R., 2001. Phase 2 early afterdepolarization as a trigger of polymorphic ventricular tachycardia in acquired long-QT syndrome. Direct evidence from intracellular recordings in the intact left ventricular wall. *Circulation* 103, 2851–2856.
- Zabel, M., Hohnloser, S.H., Behrens, S., Li, Y.-G., Woosley, R.L., Franz, M.R., 1997. Electrophysiologic features of torsade de pointes: insights from a new rabbit heart model. *J. Cardiovasc. Electrophysiol.* 8, 1148–1158.
- Zygmunt, A.C., Eddlestone, G.T., et al., 2001. Larger late sodium conductance in M cells contributes to electrical heterogeneity in canine ventricle. *Am. J. Physiol. Heart Circ. Physiol.* 281 (2), H689–H697.